NTNU – Trondheim
Norwegian University of
Science and Technology

Antenna System for Tracking of Unmanned Aerial Vehicle

Lars-Eirik Dalbakk

Electronics System Design and Innovation
Submission date: June 2014
Supervisor: Egil Eide, IET

Norwegian University of Science and Technology
Department of Electronics and Telecommunications

Summary

Target tracking is a critical part of any mobile communication system with a directive receiver antenna. Some popular tracking methods use the detected phase difference between signals received by several antennas to find the signal's direction of arrival. The measured direction of arrival is used to adjust the directive antenna's radiation pattern towards the transmitter. Thus, the radio link between the receiver and the transmitter is kept optimal at all times.

This thesis presents the design and implementation of a tracking system, that is based on the phase difference between a QPSK modulated signal received at two distinct antennas. The objective of the tracking system were to improve the existing radio link at Andøya Rocket Range, and have a range of 20 km. For this system, the direction of arrival was measured between 60° and 120° angle of arrival, allowing a maximum estimated direction of arrival error of 2°. The tracking algorithm was implemented in NI LabVIEW, with two universal software radio peripherals as receivers.

Accuracy measurements of the tracking system were taken in an anechoic chamber, for different power specifications. With a received power of -45.9 dBm and higher, the measured direction of arrival error varied between 0° to 2°, fulfilling the accuracy requirement. At a received power of -56 dBm, the error was between 2° to 7°. Although it did not fulfill the accuracy requirement, the estimation was still within the half power beamwidth of the directive receiver antenna. Thus it was defined as the lower power limit for a functioning tracking system. Assuming that there are no interference or loss due to reflections in the channel, the maximum range of the tracking system is 680 m. Hence, the range requirement of 20 km are not fulfilled.

Sammendrag

Målfølging er en viktig del av ethvert mobilt kommunikasjonssystem som bruker direktive antenner. Noen populære målfølgingsmetoder måler faseforskjellen mellom et signal som er mottatt av to eller flere antenner. Dersom faseforskjellen er kjent, kan ankomstvinkelen til signalet beregnes. For å oppnå optimal radio link mellom sender- og mottakerantennen, må strålingsdiagrammet til mottakerantennen rette seg inn etter den beregnede ankomstvinkelen.

Denne oppgaven presenterer et design av et målfølgingssystem, og hvordan det er implementert. Målfølgingssystemet er basert på å finne faseforskjellen mellom et QPSK modulert signal som er mottatt av to antenner. Hensikten med målfølgingssystemet er å forbedre en eksisterende radio link på Andøya rakettskytefelt, slik at det kan ha en rekkevidde på 20 km. Ankomstvinkelen til signalet ble målt i et område på 60° til 120°, hvor 90° er rett på mottakerantennene. Det ble stilt krav om at nøyaktigheten til målfølgingssystemet skulle være innenfor 2°. Målfølgingsalgoritmen ble implementert i NI LabVIEW, med to USRPer som mottakere.

Systemets nøyaktighet ble målt for forskjellig mottatt effekt i et ekkofritt rom. Målefeilen var på mellom 0° til 2° med mottatt effekt på -45.9 dBm og høyere. Men med en mottatt effekt på -56 dBm var målefeilen mellom 2° til 7°. Selv om målingene ikke var helt innenfor kravet, var de fremdeles innenfor 3-dB-båndbredden til mottakerantennen i kommunikasjonssystemet. Derfor ble -56 dBm mottatt effekt definert som minimumskravet for at målfølgingssystemet skulle fungere. Hvis det antas at det ikke er noe tap i signalstyrke på grunn av interferens eller refleksjoner, så er rekkevidden til systemet 680 meter. Derav ble ikke kravet om rekkevidde på 20 km innfridd.

Preface

This thesis is submitted in fulfillment of the requirements for the degree of master of science (MSc) at the Department of Electronics and Telecommunications, Norwegian University of Science and Technlogy (NTNU). The work was carried out in the period January 2014 to June 2014, under the supervision of Adjunct Associate Professor Egil Eide.

Acknowledgment

I would like to thank my supervisor Egil Eide, for giving me the opportunity to work with antennas and communication systems, and for providing me with insight to problems encountered in the thesis.

I would also like to thank Senior Engineer Terje Mathiesen, for helping me find the right equipment, and for assisting me with measurements in the anechoic chamber. And last but not least, I would like to thank my fellow students and friends for valuable input during this period. I would especially like to thank Mathias Tømmer for many enlightening conversatons.

Trondheim, Norway, June 2014
Lars-Eirik Dalbakk

Table of Contents

List of Tables

List of Figures

Abbreviations

ARR	=	Andøya Rocket Range
CPFSK	=	Continous Phase Frequency Shift Keying
DOA	=	Direction Of Arrival
EIRP	=	Equivalent Isotropically Radiated Power
FH	=	Frequency Hopping
LO	=	Local Oscillator
LNA	=	Low Noise Amplifier
MIMO	=	Multiple-Input and Multiple-Output
MUSIC	=	MUltiple SIgnal Classification
NI	=	National Instruments
PEL	=	Plane Earth Loss
PSK	=	Phase-shift keying
RF	=	Radio Frequency
SDR	=	Software Defined Radio
SNR	=	Signal-to-Noise Ratio
T-R	=	Transmitter-Receiver
UAV	=	Unmanned Aerial Vehicle
USRP	=	Universal Software Radio Peripheral
VI	=	Virtual Instrument

Chapter 1

Introduction

At Andøya Rocket Range (ARR), an unmanned aerial vehicle (UAV) is used for research, resource management, and environmental surveillance. In order to accomplish these tasks, the range of the communication link between the UAV and the ground station needs to be large. However, ARR experiences loss of signal when flying further than 5 km away from the ground station, as shown in Figure 1.1. In addition, the signal from the UAV is abruptly lost at certain locations within the 5 km range. The directive antenna at the ground station is manually directed towards the UAV, which may be the reason for loss of signal. ARR wants a method to achieve optimal radio link, which is independent of transmitted GPS coordinates, and an increase in reliable communication range to 20 km.

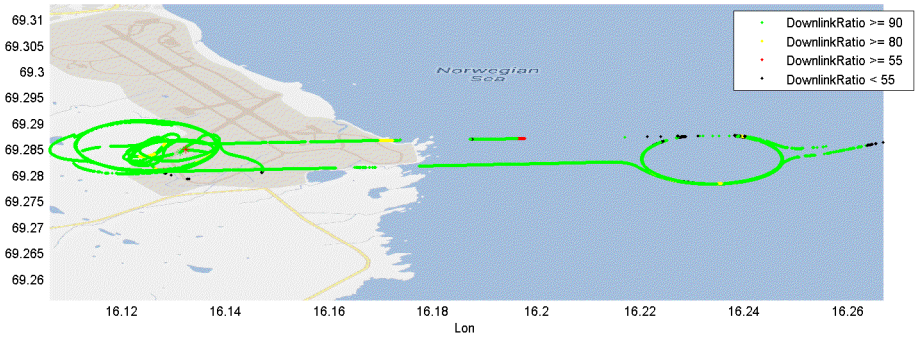

Figure 1.1: Flight pattern of the UAV. The coloured lines corresponds to the number of packages (in %) that are received at the ground station from the given locations. Loss of signal occurs at the locations where the lines ends abruptly.

The UAV is a Cruiser 2 model, shown in Figure 1.2. It is controlled from the ground by a Cloudcap Technology Piccolo 2 Autopilot [2]. A Microhard n2420 radio [3] is integrated in the autopilot, communicating with the UAV with 1 W transmit power. The antenna in

the UAV is a 2 dBi omnidirectional stub antenna.

Figure 1.2: Cruiser 2 UAV.

The radio link between the UAV and the ground is at 2.4 to 2.484 GHz. The range of the radio link is limited by the ground station antenna's gain, which is 18 dBi. Due to the high antenna gain, the radiation pattern is very directive, and must therefore be directed accurately towards the UAV. This thesis presents a tracking system of the UAV, using two extra receiver antennas. The tracking system should find the direction of the UAV in azimuth, based on the phase difference between the received signals in the two extra receiver antennas. With the direction to the UAV known, the ground station antenna can be directed automatically towards it, thus upholding optimal radio link at all times. To calculate the direction of the UAV, a software defined radio (SDR) should be used. The SDR consists of two universal software radio peripherals (USRP) and NI LabVIEW. In order to achieve an accurate enough direction estimation, a maximum estimation error of 10% of the half power beamwidth to the ground station antenna is allowed.

The main objectives of this Master's thesis are

1. Build a prototype of a tracking system by using two directive antennas, two USRPs and NI LabVIEW.

2. Demonstrate the principle of tracking and compare the achieved accuracy to the theoretical accuracy. The accuracy should be within 10% of the half power beamwidth to the ground station antenna.

3. Suggest an implementation of a system that can be used for operational tracking of UAV. The range should be 20 km.

In order to meet the objectives, several popular tracking methods were investigated with respect to theoretical performance, and complexity of software implementation. The scientific approach to implementing the software of the prototype was to experiment, test and modify known tracking methods. The accuracy of the tracking system was found by observing and measuring under controlled conditions. The suggested implementation of an operational tracking system are based on the measurements of the prototype and theoretical calculations.

1.1 Structure of the Report

The rest of the report is structured as follows; Chapter 2 gives an introduction to the theoretical background for the rest of the thesis, where the radio channel and the theoretical phase measurement errors are discussed in detail.
Chapter 3 introduces the principles of tracking, and several popular tracking methods.
Chapter 4 gives an overview of the system used at ARR, with a corresponding link budget to its radio link. It also introduces the hardware to the tracking system, and its integration in the system at ARR.
Chapter 5 describes the implementation of the tracking algorithm, along with the equipment used.
Chapter 6 is a description of how the measurements were taken, and the equipment used in the anechoic chamber. It presents and analyzes the measurements, and compares them to expected results.
In Chapter 7, the performance of the tracking system is discussed. The measurements are analyzed in detail, and put into context of the overall performance.
Finally, the thesis is concluded in Chapter 8. Recommendations for further work are also included.
The appendix contains all the calculations, figures and codes not presented in the thesis.

Chapter 2

Theoretical Background

This chapter presents the theory the rest of the thesis is based on. It gives an overview of the propagation model to the radio communication link, the sensitivity limit for a receiver system, earth bulge, and theoretical sources for measured phase errors.

2.1 The Mobile Radio Channel

The mobile radio channel places fundamental limitations on the performance of wireless communication systems. In order to correctly estimate the maximum range of the tracking system, the different types of losses in the radio channel must be accounted for.

2.1.1 Free Space Propagation

Free space path loss [4, p.107-108] is the loss a radio wave suffers when propagating in an unobstructed line-of-sight path. It is defined the difference (in dB) between the effective transmitted power P_t and the received power P_r, given by

$$PL(dB) = 10log\frac{P_t}{P_r} = -10log\left(\frac{\lambda^2}{(4\pi d)^2}\right) \tag{2.1}$$

where λ is the wavelength of the signal, and d is the distance in meters between the transmitter and the receiver. The path loss is proportional to the square of the distance d, which implies that the received power decays with distance at a rate of 20 dB/decade. The free space path loss is only valid in the far-field of the transmitting antenna, which is defined as the region beyond the far-field distance d_f, given by

$$d_f = \frac{2D^2}{\lambda} \tag{2.2}$$

where D is the largest physical linear dimension of the transmitter antenna. Additionally, to be in the far-field region, d_f must satisfy

$$d_f >> D \tag{2.3}$$

and

$$d_f >> \lambda \tag{2.4}$$

2.1.2 Multipath Fading

In addition to the direct line-of-sight path, the radio wave can arrive at the receiver through other paths due to reflection, diffraction and scattering. Those waves travels a longer distance than the direct wave, thereby causing a potential difference in phase between the radio waves. When the waves are out of phase to each other, they add up destructively at the receiver, causing a loss in signal power. This phenomenon is known as multipath fading.

Reflection

When a radio wave hits an object which has very large dimensions compared to the wavelength of the wave, part of the energy is transmitted into the object, while the rest is reflected back [4, p.114]. The energy of the reflected and transmitted waves are related to the incident radio wave by the Fresnel reflection coefficient. The reflection coefficient is a function of the material properties of the object, and generally depends on the wave polarization, angle of incidence, and the frequency of the propagating wave. Figure 2.1 shows an incident wave on a smooth surface, and its reflected and transmitted wave. The wave impinges on the surface with an angle of incidence θ_i, and is reflected by an angle θ_r and transmitted into the surface by an angle θ_t. For smooth surfaces, the angle of the reflected wave θ_r is equal to the angle of incidence θ_i as shown by

$$\theta_i = \theta_r \tag{2.5}$$

Equation (2.5) is derived from the boundary conditions from Maxwell's equations [5, p.329], and is generally known as the law of reflection.

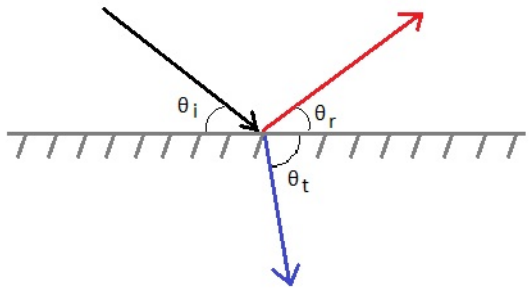

Figure 2.1: A wave impinges on a smooth surface with an angle of incidence θ_i. Part of the energy is reflected with an angle θ_r, and part of the energy is transmitted into the surface at an angle θ_t.

Diffraction

If an object with sharp irregularities obstructs the path between the transmitter and the receiver, diffraction [4, p.126] of the incident radio wave occurs. Diffraction is when a radio wave hits the edge of an object, resulting in secondary waves throughout the space and behind the object, even if there is no line-of-sight path. Diffraction depends on the geometry of the object, in addition to the amplitude, phase, and polarization of the incident wave. The diffracted waves propagates a longer distance than the direct waves, causing diffraction loss. The concept of the diffraction loss as a function of the path difference is explained by Fresnel zones [4, p.126-128].

The zones where the secondary waves have a path length from the transmitter to the receiver, which are $n\lambda/2$ longer than the path length to the direct line-of-sight signal, are called Fresnel zones. The first Fresnel zone encircles the area where the phase shift will be between 0° to 180°, while the second Fresnel zone encircles the area where the phase shift will be between 180° to 360°. Figure 2.2 shows a model of a Fresnel zone, where F_n is the radius at a given observation point P along the direct path. The distance d_1 and d_2 is the distance from each antenna to the observation point P.

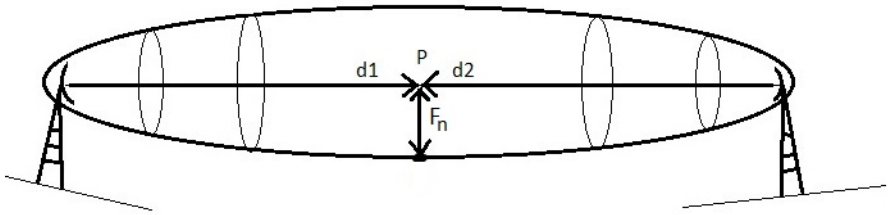

Figure 2.2: Model of a Fresnel zone with radius F_n at a given point P along the direct path between the transmitter and receiver antennas.

As shown in Figure 2.2, the radius of the Fresnel zones varies with the location of the observation point P. The radius of the nth Fresnel zone is given by

$$F_n = \sqrt{\frac{n\lambda d_1 d_2}{d_1 + d_2}} \tag{2.6}$$

where λ is the wavelength of the transmitted radio wave.

In general, if an obstruction does not block the volume contained within the first Fresnel zone, then the diffraction loss will be minimal, and diffraction effects may be neglected. In fact, a rule of thumb used for design of line-of-sight microwave links is that as long as 55% of the first Fresnel zone is kept clear, then further Fresnel zone clearance does not significantly alter the diffraction loss.

Scattering

Scattering [4, p.135] occurs when the radio wave hits a rough surface, small objects or any other irregularities, causing the reflected energy to spread out in all directions. If the dimension of the surface is much larger than the wavelength of the radio wave, the surface may be modeled as a reflecting surface. The roughness of the surface determines the propagation effects induced from the surface. Figure 2.3 shows scattering of a wave incident on a rough surface (left), and the reflection from a wave incident on a smooth surface (right). When the radio wave impinges upon a rough surface, the energy of the wave is scattered in many directions. If the surface is smooth, all the energy is reflected in one direction.

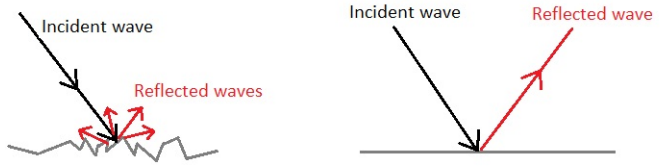

Figure 2.3: A radio wave that impinges upon a rough surface scatters in all directions. A radio wave that impinges upon a smooth surface is reflected in one direction.

The Rayleigh criterion is used to decide if a surface is smooth or rough. It states that if the minimum to maximum protuberance h is less than a critical height h_c, the surface is considered smooth. If h is greater than h_c, the surface is considered rough. The critical height h_c is a function of the angle of incidence θ_i of the radio wave, given by

$$h_c = \frac{\lambda}{8sin\theta_i} \tag{2.7}$$

where λ is the wavelength of the radio wave.

2.1.3 Plane Earth Loss Model

The plane earth loss (PEL) model [6, p.98-100] is a propagation model that describes the propagation loss for a direct line-of-sight signal in addition to its reflection from the flat reflecting ground. The situation is illustrated in Figure 2.4, where the transmitter and receiver antennas are stationed above a flat reflecting ground at height h_t and h_r respectively, separated by a distance d. The direct wave from the transmitter antenna travels a distance d_1, while the reflected wave travels a distance $d_2 > d_1$.

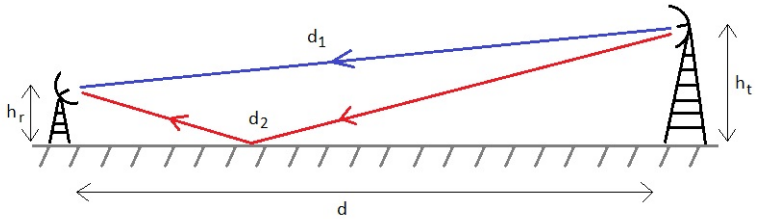

Figure 2.4: Plane earth loss model where the transmitter antenna is stationed h_t meters above the ground, and the receiver antenna is stationed h_r meters above the ground. The ground is perfectly conductive, causing all the energy of the incident wave to be reflected to the receiver. The direct wave travels a distance d_1, while the reflected wave travels a distance $d_2 > d_1$.

Assuming that the antenna heights are small compared to the total path length, and that the amplitudes of the received waves are identical apart from the Fresnel reflection loss R, the path loss PL is given by

$$PL = \frac{P_r}{P_{direct}} = \left|1 + R * exp\left(jk\frac{2h_t h_r}{d}\right)\right|^2 \tag{2.8}$$

where k is the free space wavenumber, P_r is the total received power and P_{direct} is the power received by the direct wave. Assuming that the direct wave is subject to free space loss given by Equation (2.1), the received power from the direct wave is given by

$$P_{direct} = P_t\left(\frac{\lambda}{4\pi d}\right)^2 \tag{2.9}$$

where P_t is the transmitted power. Inserting (2.9) into (2.8) gives

$$PL = \frac{P_r}{P_t} = \left(\frac{\lambda}{4\pi d}\right)^2 \left|1 + R * exp\left(jk\frac{2h_t h_r}{d}\right)\right|^2 \tag{2.10}$$

Assuming that the path length d is very large compared to the antenna heights, the angle of incidence to the ground is close to zero. Thus, given by Equation (2.7), the surface is considered smooth, and the magnitude of the reflection coefficient R will be close to unity. If it is assumed that the signal always undergoes a phase change of $180°$, then $R \approx -1$, and (2.10) can be expressed as

$$PL = \frac{P_r}{P_t} = 2\left(\frac{\lambda}{4\pi d}\right)^2 \left[1 - cos\left(k\frac{2h_t h_r}{d}\right)\right] \tag{2.11}$$

2.2 System Sensitivity Limit

Sensitivity limit expresses the lower limit of the signal power required at the receiver in order to distinguish the signal from the receiver noise. Every receiver have a given sensitivity limit for a given modulation method, and it is a function of the receiver's equivalent

noise temperature. However, the receiver's sensitivity limit does not take into account the change in the system's equivalent noise temperature due to the antenna, the transmission lines and other components such as a low noise power amplifier (LNA). In order to find the sensitivity limit of the total system seen from the receiver terminals, the receiver system effective noise temperature T_{rs} must be derived.

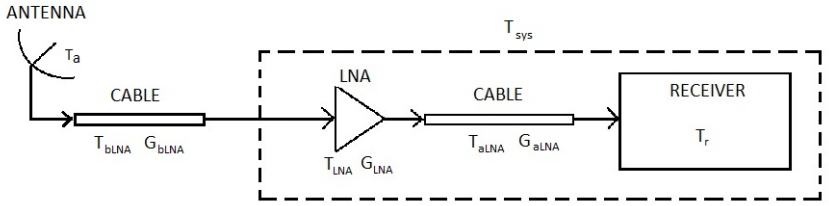

Figure 2.5: Cascade of a receiver system consisting of an antenna, a LNA, transmission lines and a receiver.

A receiver system usually consists of an antenna connected to a LNA, which is connected to a receiver by a transmission line. Figure 2.5 shows a typical receiver system, where the antenna have a antenna temperature T_a seen from the receiver terminals, the LNA have a gain G_{LNA} and a noise temperature T_{LNA}, and the receiver have a noise temperature T_r. Between the antenna and the LNA there is a transmission line with G_{bLNA} loss and T_{bLNA} equivalent noise temperature. Between the LNA and the receiver there is a transmission line with G_{aLNA} loss and T_{aLNA} equivalent noise temperature. The receiver system effective noise temperature T_{rs} is a sum of T_a, T_{bLNA} and T_{sys},

$$T_{rs} = T_a + T_{bLNA} + T_{sys} \tag{2.12}$$

Consider the cascade consisting of the LNA, the transmission line after the LNA and the receiver, shown inside the box T_{sys} in Figure 2.5. Each component has its respective gain and noise temperature. The overall noise temperature of the cascade is T_{sys}, given by

$$T_{sys} = T_{LNA} + \frac{T_{aLNA}}{G_{LNA}} + \frac{T_r}{G_{LNA}G_{aLNA}} \tag{2.13}$$

Equation 2.13 show that the noise characteristics of the cascaded system are dominated by the LNA. In order to achieve the best system noise performance, the LNA should have a low noise figure and a high gain. The noise figure of cascaded components is discussed closer in *Microwave and RF Wireless Systems*[7, p.91] by David Pozar.

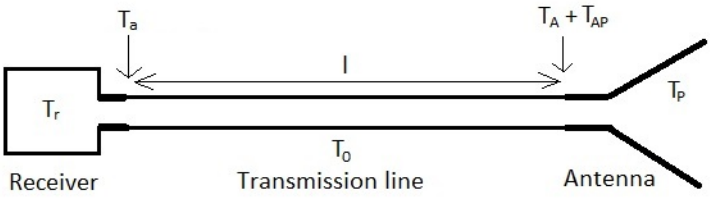

Figure 2.6: Antenna, transmission line, and receiver arrangement for system noise power calculation. (*Figure 2.35 from [1]*)

If the antenna have a physical temperature T_p and is connected to the receiver by a transmission line of length l as shown in Figure 2.6, the antenna temperature T_a seen from the receiver terminals [1, p.104] is given by

$$T_a = T_A e^{-2\alpha l} + T_{AP} e^{-2\alpha l} + T_0(1 - e^{-2\alpha l}) \tag{2.14}$$

where T_A and T_{AP} is the antenna noise temperature and the physical antenna temperature seen from the antenna terminals respectively, T_0 is the physical temperature of the transmission line, and α is the attenuation coefficient of the transmission line in Np/m, given by

$$\alpha(Np/m) = \frac{\alpha(dB/m)}{20(log_{10}e)} \tag{2.15}$$

The physical antenna temperature seen from the antenna terminals T_{AP} is given by

$$T_{AP} = \left(\frac{1}{e_A} - 1\right) T_p \tag{2.16}$$

where e_A is the thermal efficiency of the antenna. Note that all the temperatures are given in Kelvin.

Thus, with all the parts in (2.12) derived, the system sensitivity limit SL_{sys} can be found by adding the difference (in dB) between the receiver system effective noise N_{rs} and receiver noise N_r, to the receiver sensitivity limit SL_r.

$$SL_{sys}(dBm) = SL_r(dBm) + (N_{rs} - N_r)(dB) = SL_r(dBm) + \Delta N(dB) \tag{2.17}$$

where

$$\Delta N = N_{rs} - N_r \tag{2.18}$$

The system noise N_{rs} is given by

$$N_{rs} = kT_{rs}B \tag{2.19}$$

where k is Boltzmanns constant and B is the receiver bandwidth.

2.3 Earth Bulge

Earth bulge [8] is defined as the curvature of the earth between two arbitrary points, as shown in Figure 2.7. Standing at point A and looking towards point B, the earth's obstruction height h can be calculated for any point along the curvature of the earth by

$$h = \frac{d_1 d_2}{12.75k} \tag{2.20}$$

where d_1 and d_2 are the distance in meters from the obstruction point to point A and B respectively. Due to refractive effects of the atmospheric layers, radio waves do not propagate in straight lines. Instead they are slightly curved. A factor k compensates for this, and is normally chosen as $\frac{4}{3}$.

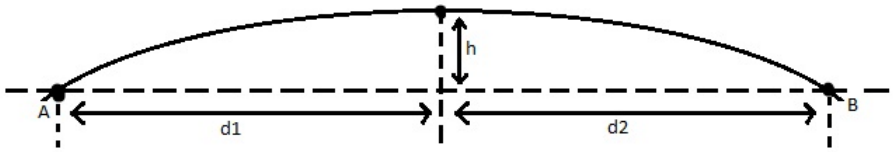

Figure 2.7: The curvature of the earth between two points A and B.

2.4 Phase Measurement Error due to Noise

When measuring the phase of a signal, errors due to noise are common. The phase error in measurements caused by the noise, is given by the phase displacement $\Delta\phi$ [9, p.70]. By assuming that the signal is sinusoidal with a power S, and that the noise power in the bandwidth is N, the phase displacement $\Delta\phi$ due to the noise can be found by

$$\sqrt{2S}cos\phi\Delta\phi = n(t) \tag{2.21}$$

where $\sqrt{2S}$ is the peak amplitude of the signal, and $n(t)$ is the noise voltage given by

$$\overline{|n(t)|^2} = N \tag{2.22}$$

By squaring and taking the time average of Equation (2.21), the phase error due to noise is given by

$$\sqrt{(\Delta\phi)^2} = 1/\sqrt{\frac{S}{N}} \tag{2.23}$$

where S/N is the signal-to-noise ratio. The phase displacement is given in radians, and must be converted to angle to find the phase angle error.

When measuring the phase differences between two signals with uncorrelated noise, the total phase displacement due to noise is given by

$$\Delta\phi_{1,2} = \sqrt{\frac{1}{(S/N)_1} + \frac{1}{(S/N)_2}} \tag{2.24}$$

where $(S/N)_1$ and $(S/N)_2$ are the signal-to-noise ratios of the measured signals.

Chapter 3

Tracking Methods

In a communication system, the receiving antennas typically need a large gain in order to fulfill large range requirements. Large antenna gain can be achieved by either using numerous antenna elements in an array, or by having a very directive antenna. The downside of using a very directive antenna is that its beamwidth is very narrow. In order to achieve an optimal radio link at all times, the radiation pattern of the antenna must be steered towards the transmitter.

This chapter introduces several methods to detect where the transmitter antenna is relative to the receiver antennas. The information can then be used to direct the radiation pattern towards the transmitter. As mentioned in Chapter 1, the direction of the transmitter should be estimated with two separate receiver antennas. All the methods introduced in this chapter are based on measuring the phase difference or time difference between the signals received at the two antennas. Phase measurements have an ambiguity of $2\pi n$, where $n = 1, 2, 3, 4, ...$ If the phase of one signal is measured as 23°, the other is measured as 57°, and the distance between the receiver antennas is unknown, then it is impossible to know if the phases are detected in the same wave. The phase difference could be 34°, or it could be 394°. It is therefore important that the distance between the two tracking antennas are less than a wavelength, to avoid the potential phase detection ambiguity.

3.1 Direction of Arrival

One method of detecting the direction of the transmitter antenna is the Direction of Arrival (DOA) method [1, p.962]. The general concept is to use two antennas or more, and measure the time delay of each received signal with respect to a reference antenna. The time delay is then used to calculate the direction of arrival.

Consider the two antennas in Figure 3.1, separated in azimuth by distance d in meters. The antennas receives a signal at the time t_1 and t_2 respectively. The signal have an angle of arrival θ, given by

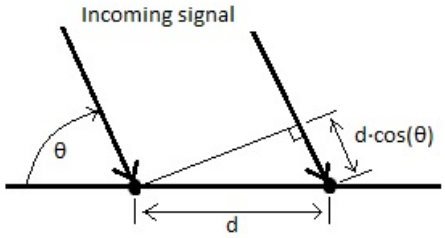

Figure 3.1: Incoming signal on two antennas separated by a distance d. (Borrowed from [1, p.966].)

$$\begin{aligned} \Delta t = t_1 - t_2 = \frac{d\cos\theta}{v_0} \\ \theta = cos^{-1}\left(\frac{v_0(t_1 - t_2)}{d}\right) \end{aligned} \tag{3.1}$$

where v_0 is the speed of light in free-space. When the signal arrives from an angle $\theta = 90°$, the transmitter is perfectly aligned between the two receiving elements. Assuming that the two antennas are just used for detecting the DOA, and that a third receiver antenna with radiation pattern towards $\theta = 90°$ are stationed directly between them for communication purposes, then $\theta = 90°$ is the optimal angle for the best possible radio link. This solution is only for one dimension though, in this case the azimuth dimension. In order to cover both azimuth and elevation, a NxM element array is needed, where $N, M = 2, 3, 4, 5, ...$

3.2 Delay-And-Sum Method

The delay-and-sum method [10, p.17], also referred to as the Fourier method, is a classical DOA detection method. It finds the time delay or phase shift between the incoming signals by use of convolution or Fourier transform. When using convolution, the sample positions of the correlated signals can be found by using a peak detector. The location of the sample with the highest peak corresponds to the sample delay between the correlated signals. Multiplying the sample delay with the sample period gives the time delay. By using Equation (3.1), the DOA can be calcualted.

The advantage of the delay-and-sum method is that it is very easy to implement, and it can be used when the signal properties are unknown. However, it offers poor performance in resolution, having an accuracy of one sample.

3.3 MUSIC

Multiple signal classification (MUSIC) [11] is a method used to estimate the frequency content of a signal or autocorrelation matrix using an eigenspace method. This algorithm

provides information about the number of incident signals, DOA of each signal, strengths and cross correlations between incident signals, and noise powers.

MUSIC outperforms simpler methods such as the delay-and-sum method when the number of incident signals is known in advance. The MUSIC algorithm uses the knowledge of incident signals to ignore the noise interference. In addition, MUSIC achieves a much better accuracy than the delay-and-sum method.

One of the drawbacks is that it requires very precise and accurate array calibration. This means that it is very sensitive to mutual coupling [1, p.966] between the antenna elements, which needs to accounted for properly. Another drawback is that, if the impinging signals are highly correlated, it fails to estimate the DOA correctly because the covariance matrix of the received signals becomes singular. And lastly, it is computationally intensive, which might be unpractical for a mobile system.

3.4 Carrier Recovery by Costas Loop

One way of detecting the phase of a signal is by using a Costas loop [12, p.57], [13, p.229]. The Costas loop is a form of phase-locked loop that measures the phase error between a coherent quadrature signal, generated in the LO, and the received signal. Generally, the phase error is used to align the quadrature signal to the received signal, in order to successfully demodulate the signal. However, the phase difference between two received signals can be found by comparing the phase errors.

The advantage of using the Costas loop carrier recovery method is that it is able to recover the unknown carrier frequency in a M-ary PSK modulated signal. Thus, shifts in frequency due to Doppler shifts [6, p.228] are not an issue. The disadvantage of using the Costas loop is that it suffers from a 360/M degree phase ambiguity when it is demodulated.

Chapter 4

System Design

This chapter introduces the communication system in use at Andøya Rocket Range (ARR), and gives an outline on how a tracking system can be integrated into it. It also evaluates the radio link of the communication system, and the corresponding radio link to the tracking system.

4.1 Receiver and Transmitter System

At ARR, an unmanned aerial vehicle (UAV) is controlled from the ground by a portable radio system. The radio is a Microhard n2420 radio [3], that is integrated in a Cloudcap Technology Piccolo 2 Autopilot [2]. The radio is designed to communicate with multiple UAVs at the same time, thus using frequency hopping (FH) over a tuning range of 2.4 to 2.484 GHz in order to avoid interference between the signals. The power spectrum of the frequency hopping signal is displayed in Figure 4.1. The signal is CPFSK modulated, with a transmitted power of 1 W and a bandwidth of 210 kHz.

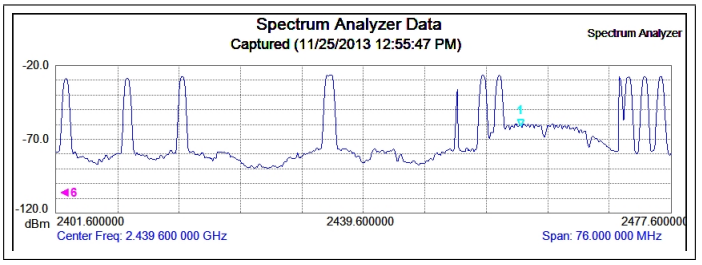

Figure 4.1: Power spectrum of received signal with Microhard n2420 radio. Displays the power spectrum of a FH mode over the tuning range.

For simplicity, the portable radio system at the ground will be referred to as the receiver

system, and the radio system in the UAV will be referred to as the transmitter system.

The antenna in the receiver system is a 18 dBi reflector antenna [14], with approximately 20° beamwidth. It operates at 2.4 - 2.485 GHz, and is vertically polarized. The diameter of the antenna is 45.8 cm, the depth is 12 cm, and it weighs 1.7 kg. The transmitter antenna in the UAV is a 2 dBi quarter wavelength stub antenna [15]. It is connected vertically to a ground plane at the bottom of the UAV, directed downwards, and it is vertically polarized. Figure 4.2a and 4.2b shows the receiver antenna and the transmitter antenna.

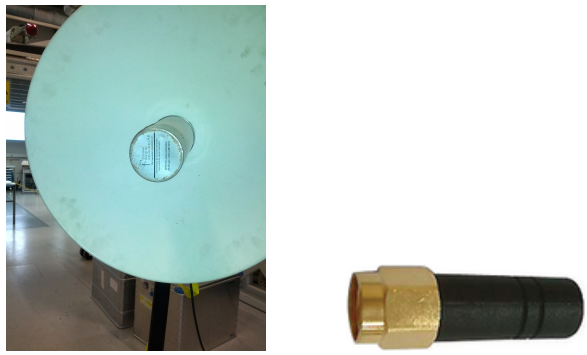

(a) • **(b)** •

Figure 4.2: a) 18 dBi reflector antenna at receiver system. **b)** 2 dBi quarter wavelength stub antenna in the UAV.

At ARR, the receiver antenna is manually steered towards the UAV. In order to optimize the radio link, two independent antennas should be used to detect the direction of arrival (DOA) of the signals from the UAV. The receiver antenna in the communication system is then adjusted accordingly, ensuring that its radiation pattern is always directed towards the UAV. To avoid confusion, the independent antennas used for DOA detection will be referred to as the tracking antennas, and the receiver antenna in the communication system will be referred to as the main receiver antenna. The tracking antennas are 9 dBi directional antennas [16], with 60° beamwidth in H-plane and 76° beamwidth in E-plane. The antennas are vertically polarized, and are 120 mm wide and 120 mm long. The tracking antennas are displayed in Figure 4.3.

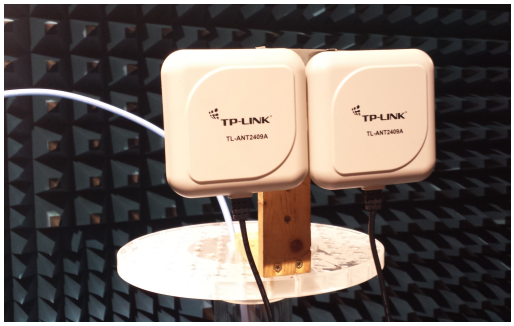

Figure 4.3: The 9 dBi tracking antennas used for DOA estimation.

As mentioned above, the purpose of the tracking antennas is to detect the DOA of the signal in order to adjust the main receiver antenna in the right direction. Therefore, the tracking antennas need to be directed in the same direction as the receiver antenna, and adjusted along with it. One way of achieving this is by mounting the tracking antennas on a rotating platform, with the main receiver antenna mounted on top of them, as shown in Figure 4.4. The center of the tracking antennas are separated by a distance d, which should be shorter than a wavelength in order to avoid phase detection ambiguities. The antennas are connected to their respective receivers that estimate the DOA. The estimated DOA is then used to rotate the platform, and thus the antennas, in the direction of the signal.

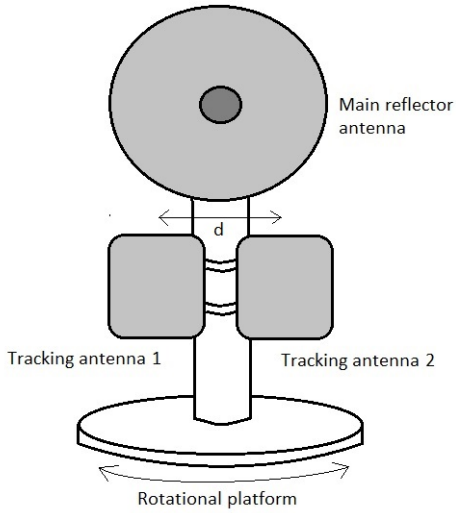

Figure 4.4: Setup of receiver antennas in a tracking system. The tracking antennas estimates the direction of arrival, which is used to rotate the platform such that the main reflector antenna has its radiation pattern towards the transmitter.

4.2 Signal Propagation and Link Budget

As mentioned in Chapter 1, the range requirement of the radio link is 20 km. In order to estimate the quality of the radio link correctly, the signal attenuation and all the loss specifications must be derived. Some specifications of the radio link have already been presented in Chapter 4.1, and are displayed in Table 4.1

Table 4.1: Radio link specifications

Transmit power	1 W
Frequency tuning range	2.4 - 2.484 GHz
Signal bandwidth	210 kHz
Modulation technique	CPFSK
Range requirement	20 km
Transmitter antenna gain	2 dBi
Main receiver antenna gain	18 dBi
Tracking antenna gain	9 dBi

To estimate the signal attenuation, all the obstructions in the signal path must be accounted for. The UAV usually fly above the ocean, where the main receiver antenna have a direct line-of-sight to the horizon. Therefore, no physical obstructions such as trees and buildings exists, which can cause scattering of the signal. The only obstruction of consequence is the ocean, since it either scatters or reflects the signal. In the worst case scenario, the UAV flies beyond the horizon, out of line-of-sight. In order to determine if the antenna have a direct line-of-sight to the UAV within the range requirement, the earth bulge [8] must be calculated. The reflector antenna is stationed 10 meters above the ground, while the UAV is flying minimum 100 meters above the ground. By inserting the antenna heights into Equation (2.20), the earth bulge has been calculated at any point between the transmitter and receiver. Figure 4.5 shows the clearance of the first Fresnel zone [4, p.126-128], given the height specifications. The clearance of the first Fresnel zone is the distance from the ground to the first Fresnel zone at any given point. Therefore, it is clear from Figure 4.5 that the earth bulge does not obstruct the first Fresnel zone. According to Rappaport [4, p.129], if 55% of the first Fresnel zone is free of obstructions, it can be assumed that the RF signal propagates as in free space. Hence, it can be assumed that the direct line-of-sight signal suffers only from free space path loss [4, p.107-108].

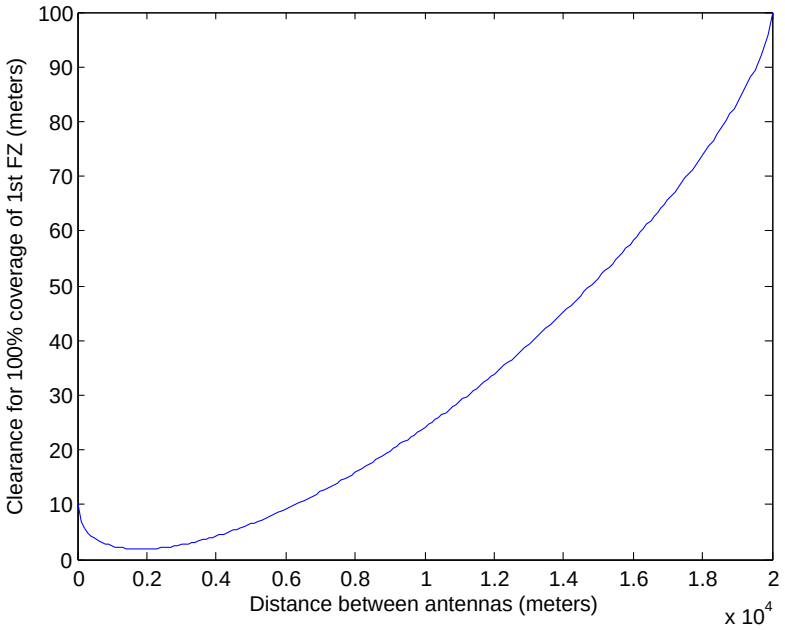

Figure 4.5: 100% Clearance of First Fresnel Zone.

Although the direct signal propagates as in free space, the signal arrives at the receiver from other directions as well. The sea can cause scattering or reflection of the signal, due to its waves. According to Rappaport [4, p.135], a surface is considered smooth if its minimum to maximum protuberance h is less than h_c, given by Equation (2.7). Thus, when the total path length (20 km) is much greater than the heights of the antennas (10 m, 100 m), the surface is considered smooth, since the angle of incidence is close to grazing the ground. As the surface is considered smooth, it can be assumed that the signal arrives at the receiver from a direct path and from a surface reflection.

For this type of signal propagation, the plane earth loss (PEL) model [6, p.98-100] derived in Chapter 2.1.3 is a good approximation of the propagation loss. Figure 4.6 shows the theoretical PEL calculated from Equation (2.11) by inserting the height of the antennas. In general, the loss increases by 20 dB per decade for relatively short distances, and 40 db per decade for large distances. However, the reflection cancels out the direct signal at specific locations, causing the signal to drop in power. These locations are displayed as troughs in Figure 4.6. Often a slight decrease or increase of range gives a much more acceptable path loss.

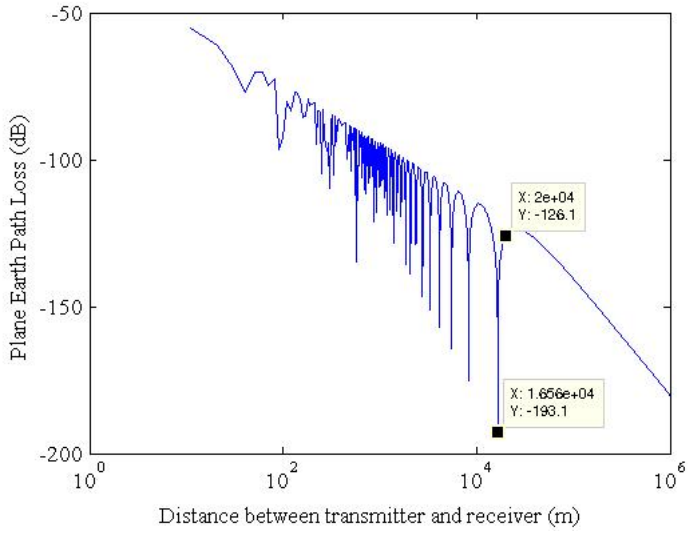

Figure 4.6: Plane earth loss between transmitter and receiver stationed 100 and 10 meters above the ground respectively. The signal is propagating at 2.484 GHz

Based on the specifications in Table 4.1 and the choice of propagation model, a link budget has been developed in Table 4.2 for the radio link to the main receiver antenna. The carrier frequency was chosen as 2.484 GHz, since it is the frequency in the tuning range that leads to the largest path loss. Using the values from Table 4.1, the PEL is calculated as 126.1 dB, as shown in the appendix. In addition to PEL, the budget accounts for polarization loss due to difference in the polarization of the antennas. Polarization loss occurs when the antennas are not properly aligned and/or when the environment distorts the received polarization. This is bound to happen in some degree, and to account for a loss due to polarization misalignment, the system budgets a loss of 10% in received power. This corresponds to a loss of 0.46 dB, and a misalignment of 18.4° (in an isolated environment). Interference from other wireless systems are unlikely, considering that the flight operations takes place in a remote area. Therefore it has not been included in the link budget.

Table 4.2: Link budget for the radio link with the 18 dBi reflector antenna as the receiving element

Link Budget	**Input**	**In dB**
Transmitter:		
Transmit power	1 W	0 dBW
Antenna gain		2 dBi
EIRP		**2 dBW**
Propagation:		
Carrier frequency	2.484 GHz	
Distance	20 km	
Plane Earth Loss		126.1
Polarization loss		0.5
Total Propagation Loss		**126.6**
Receiver:		
Antenna gain		18 dBi
Received power		-76.6 dBm
LNA gain		13
LNA noise figure		1.1
LNA noise temp	83.6 K	
Cable loss before LNA		0.0
Equivalent cable noise temp before LNA	1.5 K	
Cable loss after LNA		2.3
Equivalent cable noise temp after LNA	202.5 K	
Antenna temp seen from receiver terminals	208 K	
Receiver noise figure		5
Equivalent receiver temp	627.1 K	
System noise temp	147.1 K	
Receiver system effective noise temp	356.7 K	
Receiver noise in BW		-149.9
C/N		**43.3**
Specifications:		
Receiver sensitivty limit		-105 dBm
Receiver noise N_r		-147.4
System noise N_{sys}		-149.9
Change in sensitivity due to change in noise		-2.5
System sensitivity limit		-107.5 dBm
Link Margin		**30.9**

At ARR, a low noise amplifier (LNA) is connected to the receiver antenna by a 0.1 meter long H1000C1 [17] coaxial cable. The LNA gain is 13 dB, and its noise figure is 1.1. The other end of the LNA is connected to the receiver by a 10 meter long H1000C1 coaxial cable. Long cables are necessary at ARR for practical purposes, while the LNA is introduced in order to amplify the received signal and reduce the overall system noise temperature. The H1000C1 coaxial cable has a loss characteristic of 0.23 dB/m at 2.4 GHz, and the receiver [3] ha a noise figure that is equal to or less than 5 dB. The sensitivity limit of the

receiver is -105 dBm. However, as explained in Chapter 2.2, the system's noise temperature is different than the receiver's noise temperature. Therefore, a new sensitivity limit has been calculated by Equation (2.17) as -107.2 dBm. The calculations can be found in Chapter 8.1.

With 1 W transmitted power, transmitter antenna gain of 2 dBi, receiver antenna gain of 18 dBi and 126.6 dB total loss in the channel, the received power is -76.6 dBm at a range of 20 km. With a total cable loss of 2.3 dB, and 208 K antenna temperature at receiver terminals, the signal to noise ratio (SNR) is 43.3 dB. Accounting for the change in sensitivity limit, the link margin to the radio link is 30.9 dB. Although the margin is good, it is important to remember that the PEL increase drastically at specific locations between the transmitter and receiver, which will likely cause a negative link margin, and thereby loss of signal.

The radio link has been evaluated for the communication system with the main receiver antenna, and by ignoring the sudden drops in signal power due to reflections, the link margin is sufficient to receive signals reliably for ranges up to 20 km at the very least. However, for the communication system to have an optimal radio link, the tracking system need to fulfill the range requirement as well. Thus, a link budget with the tracking antennas as the receiving elements has been developed. Its main purpose is to see if the radio link with tracking antennas can achieve a good enough link margin at 20 km range. Most of the specifications and propagation effects mentioned above are the same in order to make the link budget as close as possible to the conditions at ARR. However, certain specifications are different. For instance, the gain of the tracking antennas is 9 dBi, and the radios are replaced with universal software radio peripherals, which are software defined radios (more on this in Chapter 5.1). The link budget of the radio link is displayed in Table 8.1 in the appendix, but the most important properties have been summed up in Table 4.3. Comparing the properties from the tracking antenna radio link with the properties from the main receiver antenna radio link, it is shown that the received power, the SNR and the link margin is 9 dB smaller. This is the expected result, since the only change of real consequence is a reduction in receiver antenna gain of 9 dB. The link margin is 21.9 dB at a distance of 20 km, which is seemingly good. However, this radio link has the same issue as the one with the main receiver antenna. At specific locations, the signal drops in power, causing the antennas to loose track of the UAV.

Table 4.3: The most important properties of the radio links to the main receiver antenna, and the tracking antenna in real environment.

Link Budget Properties	**Main Receiver Antenna Radio Link**	**Tracking Antenna Radio Link in Real Environment**
Transmit power	1 W	1 W
Transmitter gain	2 dBi	2 dBi
Carrier frequency	2.484 GHz	2.484 GHz
Signal bandwidth	210 kHz	210 kHz
Propagation distance	20 km	20 km
Propagation loss	126.6 dB	126.6 dB
Receiver gain	18 dBi	9 dBi
Received power	-76.6 dBm	-85.6 dBm
C/N	43.3 dB	34.3 dB
Link Margin	**30.9 dB**	**21.9 dB**

Chapter 5

Software Development

Different tracking methods have been introduced, and the radio link and its properties have been derived. This chapter covers the software implementation of one of the tracking methods, and the equipment used.

5.1 Equipment and Tools

In this thesis, software defined radios (SDR) are used for DOA estimation. An SDR is a communication system in which components such as modulators/demodulators, mixers, filters, detectors, and amplifiers are implemented in software. The SDRs used in this thesis are composed of radio frequency (RF) boards, universal software radio peripherals (USRP) and National Instruments (NI) LabVIEW.

A USRP is a general purpose, programmable hardware that allows computers to function as software radios. It performs high speed signal processing operations such as ADC/DAC, digital up/down conversion and filtering. In this thesis, two USRPs are used as receivers in the tracking system. They are of the model USRP2 [18], the second version of a series of USRP devices. The USRP2 features two 100 MS/s 14-bit analog to digital converters, and two 400 MS/s 16-bit digital to analog converters. Its configurations and firmware are stored in a secure digital flash card, and multiple USRP2 systems can be connected together to form fully coherent multiple antenna systems for multiple-input and multiple-output (MIMO). The USRP2 is connected to the host PC using the GB Ethernet interface. Figure 5.1a displays the USRP2.

The RF boards are the RF interfaces for the USRP, where the transmit power and the center frequency is tuned in LabVIEW. The RF board used in this thesis is the XCVR2450 [19], with 20 dBm maximum output power and 2400-2500 & 4900-5900 MHz frequency range. Figure 5.1b displays the RF board XCVR2450.

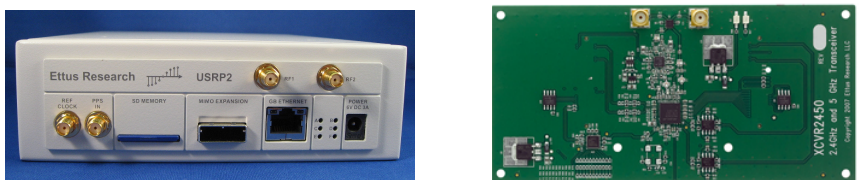

(a) • **(b)** •

Figure 5.1: a) Ettus Research USRP2. **b)** RF Daughter Board XCVR2450 in the USRP2.

NI LabVIEW [20] is a graphical programming language developed by National Instruments, that uses icons instead of text to create programs. A LabVIEW program is called a virtual instrument (VI). It has two main parts, the front panel and the block diagram. The front panel is used for user interactions and display of results, whereas the block diagram is the source code constructed in LabVIEW's graphical programming language, 'G'. The 2013 SP2 version has been used in this thesis.

5.2 Software Design Setup

In the design of the software, two test setups were used to verify that the software functioned correctly. The general idea of the test setups was to feed the same signal to the two USRPs by cables, where one of the signals was slightly out of phase to the other signal.

In the first test setup, the signal fed to the USRPs was a sine generated by a signal generator. At the generator output port, the signal was divided by an ohmic power splitter. One part was fed to a USRP through an adjustable phase shifter, while the other part was fed directly to the second USRP. Figure 5.2 shows the setup, where the signal generator is in the top right corner, the USRPs are to the left, and the adjustable phase shifter is in the bottom right corner. The cables used to connect the equipment were 30 cm long RG 223/U [21] coaxial cables. The part of the power divided connected directly to one the USRPs are connected by two cables. This is done to compensate for the two cables required to connect the other part of the power divider to the other USRP. The USRPs were connected together by a MIMO cable, where only one of the USRPs, the master, was connected to the host PC by a GB Ethernet cable. The signal from the other USRP, the slave, are then passed through the master device to the computer, along with the signal from the master. This caused the signals to be clocked to the same local oscillator (LO), and therefore be in sync. For more information on how to connect the USRPs to the computer, check the device manual [22].

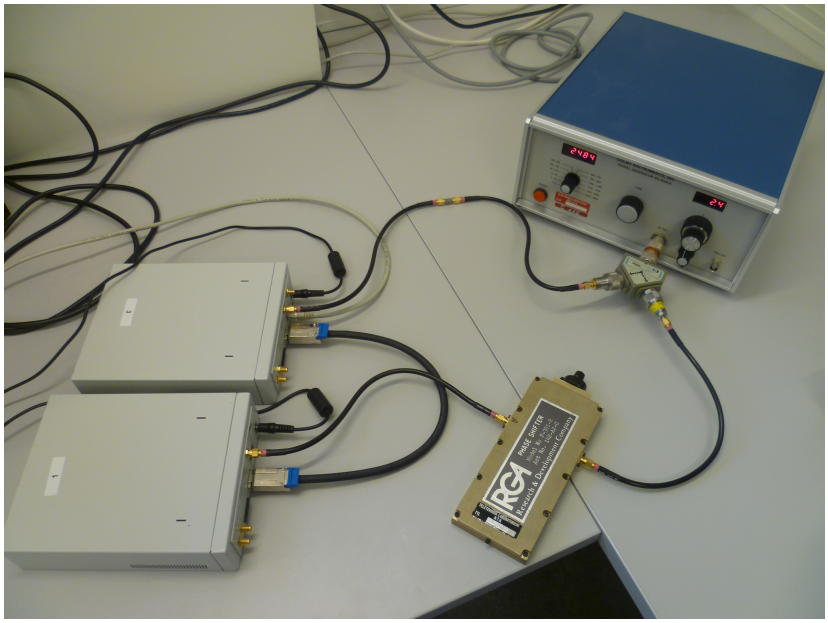

Figure 5.2: Test setup 1: The signal fed to the USRPs (to the left) is generated in the signal generator (top right corner). The signal is divided by a power splitter, where one of the ports is connected through an adjustable phase shifter (bottom right corner)

In the second test setup, the signal fed to the USRPs was a QPSK modulated bit stream generated in LabVIEW by another PC. The signal was transmitted by a third USRP2 that was connected to the power splitter by a 30 cm Sucoflex 104P coaxial cable [23]. As shown in Figure 5.3, the rest of the setup was identical to the first test setup.

The two test setups were nearly identical, only the type of signal used was different. The reason why a pure sine wave was used in the first test setup, is because it was easier to find the phase of it. By using a simple signal, it is easier to verify that the ground work of the code works appropriatly. Once the basic code was designed and verified, more complex details were added to it. At ARR, the radio uses CPFSK modulation and frequency hopping over a frequency range of 2.4 to 2.484 GHz. However, in order to limit the complexity of the thesis, it was decided that the tracking system should be created with respect to WiFi signals. WiFi systems generally uses OFDM, where each sub-channel is modulated by BPSK, QPSK or QAM. Thus, to resemble a WiFi signal, the signal chosen for the second test setup was a QPSK modulated bit stream. Table 5.1 shows all the equipment used for software development in both test setups.

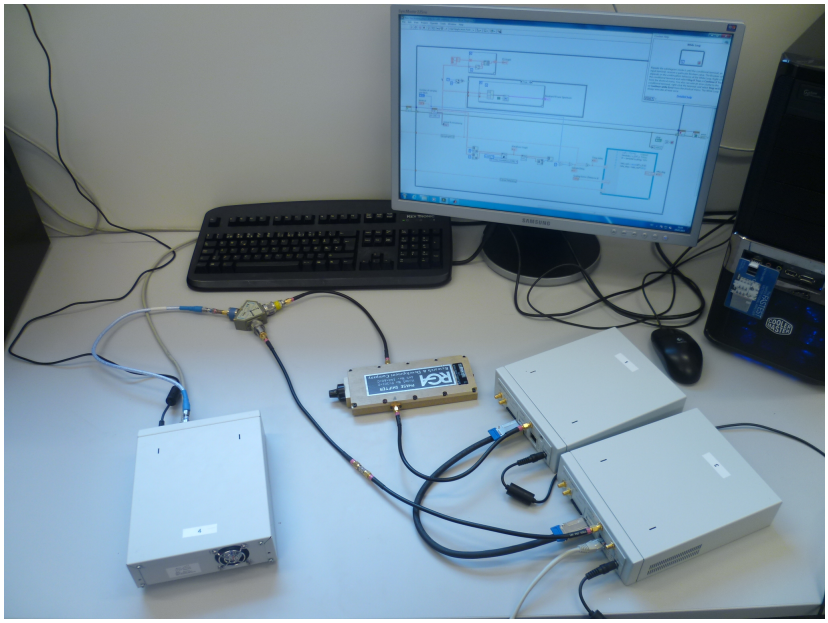

Figure 5.3: Test setup 2: A QPSK modulated signal, generated in a host PC, is fed through a USRP (on the left) to the other USRPs (on the right). The signal is divided by a power splitter, where one of the ports is connected through an adjustable phase shifter. The signals are thereby sent to the receiver host PC, that determines the phase difference between the received signals.

Table 5.1: Software development equipment

Instruments and Components	Test bench 1	Test bench 2
SG-8000A Signal Generator	x	
USRP2, snr 1147	x	x
USRP2, snr 1148	x	x
USRP2, snr 1149		x
11667A Power Splitter	x	x
P-301-R Phase Shifter	x	x
CL2 Madison MIMO Cable	x	x
RG 223/U Coax Cables	x	x
LabVIEW V.2013 SP2 (32-bit)	x	x
XCVR2460 RF board	x	x

5.3 Choice of Tracking Method

Chapter 3 introduced several tracking methods, the DOA algorithm, the sum-and-delay method, the MUSIC algorithm, and carrier recovery with Costas loop.

The sum-and-delay method [10, p.17] is very easy to implement, but it suffers a major flaw for this type of system; the best achievable resolution is one sample. The USRP2 have an input sampling rate of 100MS/s, which gives a resolution of 10^{-8} sec in the time domain. Since the carrier frequency is 2.484 GHz, variations in signal happens at a rate of approximately $4 * 10^{-10}$ sec. The signal phase changes to much from one sample to another sample, to be measured accurately enough. Therefore, the sample rate of the USRP2 is not large enough for the sum-and-delay method.

The MUSIC algorithm [11] is able to estimate the phase with an accuracy higher than one sample. It is generally a very popular method, and several different versions of it have been developed. However, MUSIC requires very precise and accurate array calibration. The two directional antennas used for tracking will affect each other with mutual coupling [1, p.966], which has not been accounted for in the thesis. Mutual coupling will therefore lead to phase detection errors if not compensated for. The MUSIC algorithm is also computationally intensive, which might be impractical for a portable system.

Carrier Recovery with Costas loop [12, p.57], [13, p.229] is arguably the best method to estimate the phase difference of PSK modulated signals. It estimates and compensates for frequency and phase differences in the carrier wave. In a PSK modulated signal, the power is spread out over a large frequency spectrum, which makes it unpractical to detect the phase of the carrier wave for other methods. However, the Costas loop uses a coherent quadrature signal to measure the phase error, thus recovering the carrier signal. One of the drawbacks is that it is sensitive to a 360/M degree phase ambiguity, where M denotes the PSK order. Hence, a QPSK signal is sensitive to a 90° phase ambiguity.

The Carrier Recovery with a Costas loop would ideally be the best method for this system. However, due to time restrictions, it was not implemented. Instead, the DOA method [1, p.962] was implemented. In order to detect the phase difference of the PSK signals, a set of bandpass filters were used to acquire the carrier frequency. Since the signal is PSK modulated, the power is spread out in the spectrum, and not focused on the carrier frequency. Therefore, it is harder to detect the phase with this method than with a Costas loop. In addition, the carrier frequency must be known beforehand. Thus, frequency shifts in the channel caused by Doppler shifts [6, p.228] may cause the filter to remove the carrier frequency. Despite these drawbacks, the DOA method was implemented because it was relatively easy to implement, and because of time restrictions.

5.4 LabVIEW Code

Up to now, the hardware and system setup for implementing the code have been presented. It was also discussed briefly why the DOA algorithm was implemented. This section presents the actual implementation of the software, before evaluating the performance of the finished code.

5.4.1 Code Overview

The objective of the tracking code is to estimate the angle of arrival of a signal. The signal is received by two antennas, and the estimation is based on the detected phase difference between the signals.

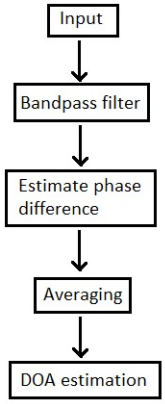

Figure 5.4: Block diagram of the tracking code

Figure 5.4 displays a block diagram of the tracking code. The *Input* block contains the received signals, which are represented as data streams of complex numbers. The data streams are passed through the *Bandpass filter* block, which is a bandpass filter with the purpose of narrowing down the signal to the carrier frequency. The carrier frequency is a sine, which is easy to find the phase to. In order to find the phase difference in the *Estimate phase difference* block, the filtered data streams are converted from rectangular form to polar form by

$$\begin{aligned} z &= a + jb = r\angle\theta \\ r &= \sqrt{a^2 + b^2} \\ \theta &= arctan\left(\frac{b}{a}\right) \end{aligned} \tag{5.1}$$

where r is the amplitude, and θ is the phase angle of the signal. Once the phase angles of both the signals are calculated, the phase difference is sent to the *Averaging* block, that

returns the phase difference averaged over one second. The last block, *DOA estimation*, converts the averaged phase difference $\Delta\theta$ to a time delay Δt, given by

$$\Delta t = \frac{\Delta\theta}{360 f_c} \tag{5.2}$$

where f_c is the carrier frequency. The time delay is then inserted into the DOA algorithm, given by Equation (3.1), that returns the estimated angle of arrival.

5.4.2 Code Implementation

National Instruments have released LabVIEW examples of transmitters and receivers. One of these examples, *niUSRP EX Rx Multiple Synchronized Inputs*, receives the synchronized signals from two USRPs connected together by a MIMO cable. The signals are sampled by an IQ rate of 2 MS/sec, before the samples are fetched from the channel and returned as an array of complex, double-precision floating-point data. This example is the foundation of the tracking code, and the complete VI of the example can be found in Figure 8.1 and 8.2 in the appendix . A complete VI of the finished tracking code can be found in Figure 8.3 and 8.4 in the appendix.

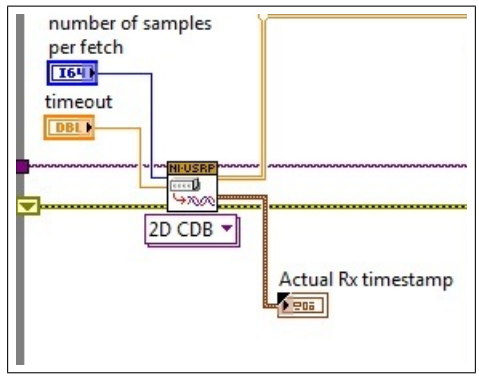

Figure 5.5: The *2D CDB* block fetches samples from the channels containing the synchronized signals, and returns an array of complex, double-precision floating-point data

One of the biggest challenges with implementing the system in LabVIEW was to keep track of the data flow. Mainly, this was an issue of the *niUSRP Fetch Rx Data (2D CDB)* block shown in Figure 5.5. The block is inside a loop, where it fetches at certain number of samples from the channels each iteration, and returns them as complex data. Whenever the block tries to fetch more samples than available in the channels, an underflow error occurs. If the block fetches too few samples, the memory in the USRP fills up, causing an overflow error. The underflow error was fixed by increasing the transmission rate, and by adjusting the number of samples per fetch to 16384 S/sec. To avoid the overflow errors, the data stream from the fetch block was inserted into a queue. The data stream was then dequeued in another loop for DOA estimation. In LabVIEW, the loops iterates simultaneously and independently of each other, as long as there is enough computational power in

the host computer. Thus, the fetch data loop was not slowed down by the DOA estimation, avoiding overflow errors in the USRP.

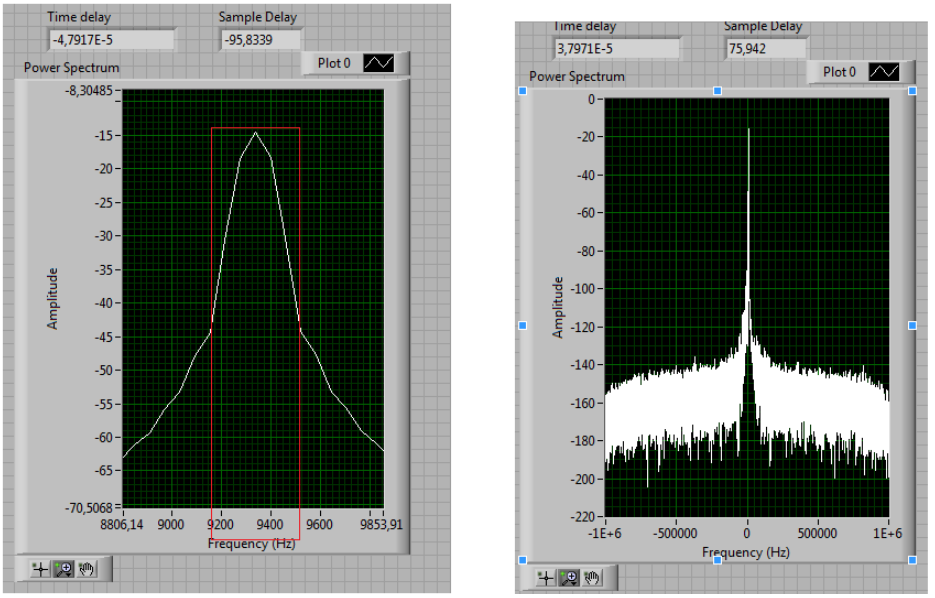

Figure 5.6: Power spectrum of the sinus signal generated by the signal generator in LabVIEW. The signal is transmitted over a coax cable with a 2.484 GHz carrier frequency. The area in the red box marks the occupied bandwidth of the signal

As explained in Chapter 5.2, two different test setups were used under the code implementation. The first test setup was used to begin with, where the signal generator generated a sinus signal, and sent it to the two USRPs by cables. Although the sinus signal already is in the wanted form, the bandpass filter was implemented for the final code. The correct filter attributes were found by looking at the power spectrum of the sine, displayed in Figure 5.6. The graph to the left is a scaled version of the total power spectrum, shown in the graph to the right. A red box containing a portion of the received power indicates the occupied bandwidth of the signal. Occupied bandwidth [24] is the bandwidth that contains 99% of the total power in the spectrum. Since the power of the sine is focused in the carrier frequency, it is safe to assume that the occupied bandwidth contains the downsampled carrier frequency. Hence the bandpass filter was implemented as a second order Chebyshev filter, with 9200 Hz low cutoff frequency, and 9500 Hz high cutoff frequency, shown in Figure 5.7.

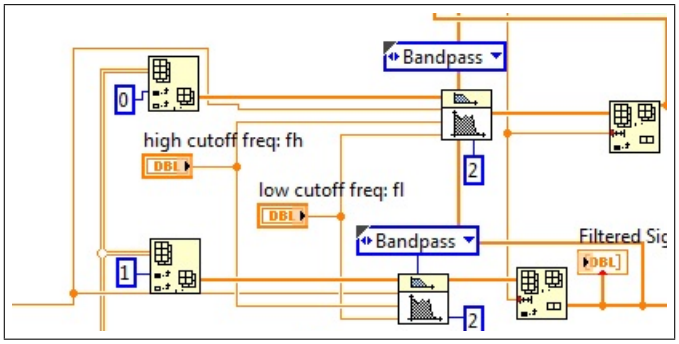

Figure 5.7: LabVIEW code of the second order Chebyshev bandpass filters

To verify that the filter specifications were correct, a QPSK modulated signal was transmitted to the USRPs. The signal was generated in LabVIEW using the example VI *niUSRP EX PSK Tx.vi*. The block code and front panel of the example is displayed in Figure 8.5 and Figure 8.6 in the appendix. Figure 5.8 shows one of the QPSK modulated signals after bandpass filtration, where the filtrated signal is in the form of a sine.

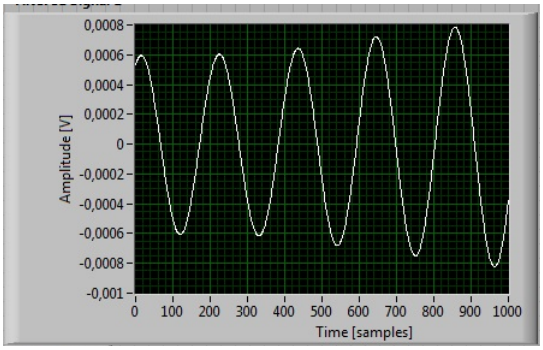

Figure 5.8: QPSK modulated signal filtered by a bandpass filter at the carrier frequency

After the signals are reduced to a sine, they are passed on to an integrated MATLAB code, shown in Figure 5.9. The MATLAB code calculates the phases of the signals by converting the data from rectangular form to polar form, by using the inbuilt MATLAB function *angle()*. *Angle()* returns the phase angle of the input in radians, which is converted to degrees in line 7 of the MATLAB code. The inputs to the MATLAB code are the filtered signals $m1$ and $m2$, the synchronization parameter $sync$, and the recursive parameters $send$ and xc.

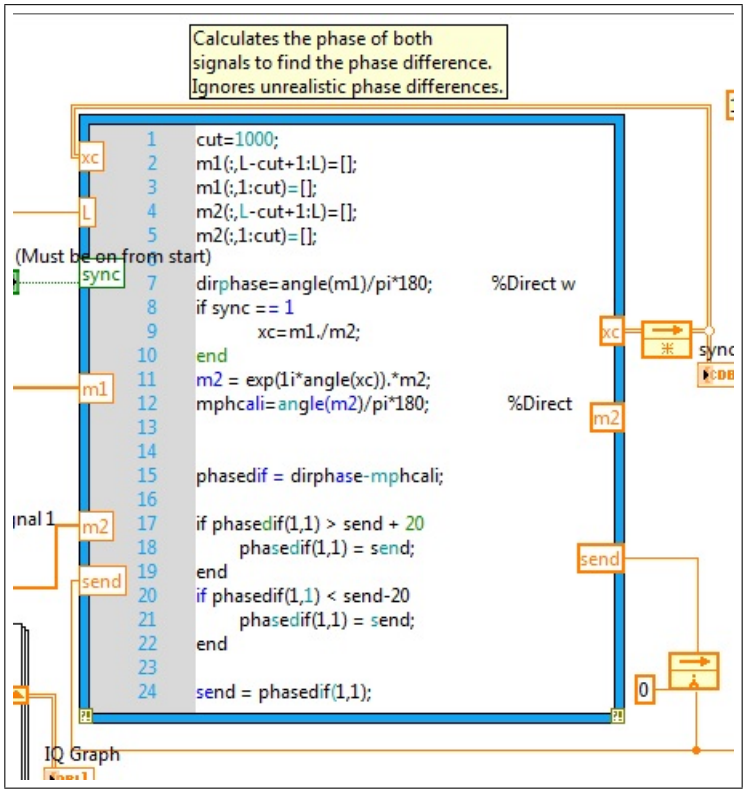

Figure 5.9: Integrated MATLAB code of the phase difference between the signal inputs $m1$ and $m2$

The synchronization parameter is a boolean switch that is controlled by the user in the front panel. When the switch is on, line 9 in the MATLAB code is executed. The recursive parameter xc is the phase difference between the input signals, that is used to adjust the phase of the $m2$ input signal. When the boolean switch is turned off, xc remains constant for each iteration of the code, providing a constant phase adjustment to $m2$. The phase adjustment is necessary because phase ambiguities occurs when the local oscillator is derived on each USRP from the reference clock. Each time a new set of data is collected, the phase difference between the signals changes because of the ambiguity. In order to compensate for the ambiguity, it is assumed that phase difference is zero when the tracking begins. By this assumption, the phase of $m2$ is adjusted by xc to make it equal to the phase of $m1$. When the signals have equal phase, the boolean switch is turned off and the calibration is completed. For this calibration to work, it is important that the angle of arrival is exactly 90° until the calibration is completed.

The phase difference is calculated in line 15 by subtracting the adjusted phase of $m2$ from the phase of $m1$. Since the filtered signals are not ideal sines, the phase difference of some samples might vary a lot from the phase difference of the surrounding samples. Assuming that the transmitter is relatively far away from the receivers, spontaneous change in phase

difference should not occur. If the current phase difference is 20° larger or smaller than the previous phase difference, then the current phase difference is equalled to the previous by line 17-22.

The MATLAB code have one additional input, L. L is the sample length of the signals after the filter, that can be adjusted by the user in the front panel. Line 1 to 5 removes the 1000 first and the 1000 last samples of the signals, in order to reduce the iteration time of the code. An overflow or underflow error could occur in the queue as well, so to make sure that the queue is emptied fast enough, L is chosen as 3000.

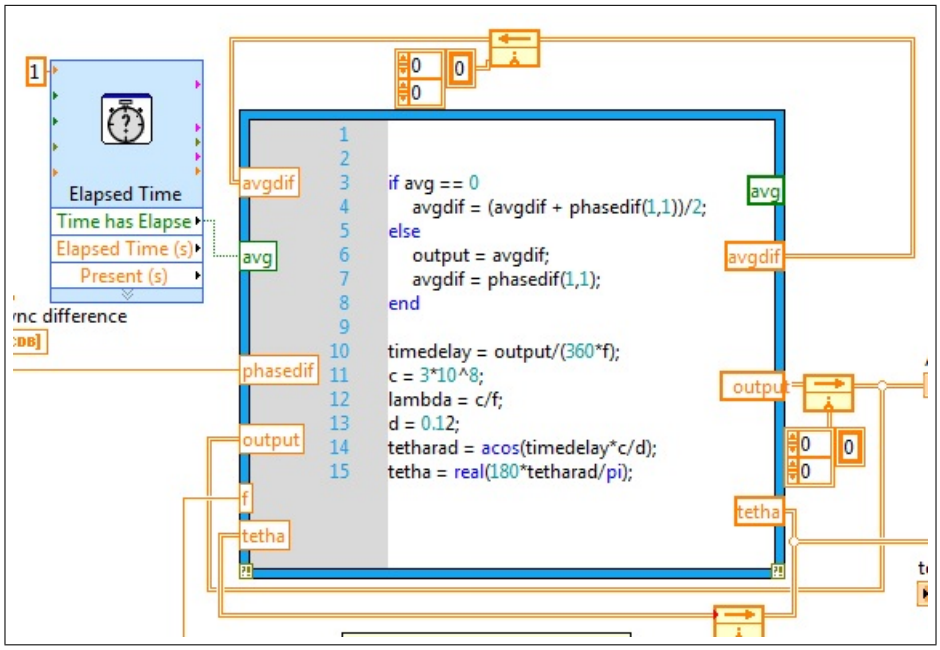

Figure 5.10: LabVIEW code of the MATLAB script performing averaging of the phase difference and calculation of DOA

The next step in the LabVIEW code is the averaging of the phase difference, and the DOA estimation. Figure 5.10 shows how the averaging and DOA estimation is done in LabVIEW, by use of an integrated MATLAB script. The $phasedif$ input is the phase difference calculated in the previous MATLAB script. The avg input is a boolean parameter from the $ElapsedTime$ block. Every time one second have passed, the avg output from the $ElapsedTime$ block is true, or have the value 1. Otherwise it is false, which equals 0. If avg is false, a recursive parameter $avgdif$ averages the current $phasedif$ input with the previous $avgdif$, displayed in line 3 to 8 in the MATLAB script. If avg is true, a parameter $output$ is given the value of $avgdif$, and $avgdif$ is reset to the current $phasedif$ value. Thus, $output$ is the one second averaged value of the phase difference, and it is converted into a time delay in line 10. Line 14 to 15 calculates the DOA in degrees, based

on the time delay by using Equation (3.1).

In addition to the block diagram with the actual code, LabVIEW features a front panel. The front panel allows the user to enter inputs such as the number of acquired samples, carrier frequency, start trigger time and IQ rate. It also displays the outputs, such as waveform graphs of the signal. Figure 5.11 displays the system front panel, showing all the controls and indicators of the finished code.

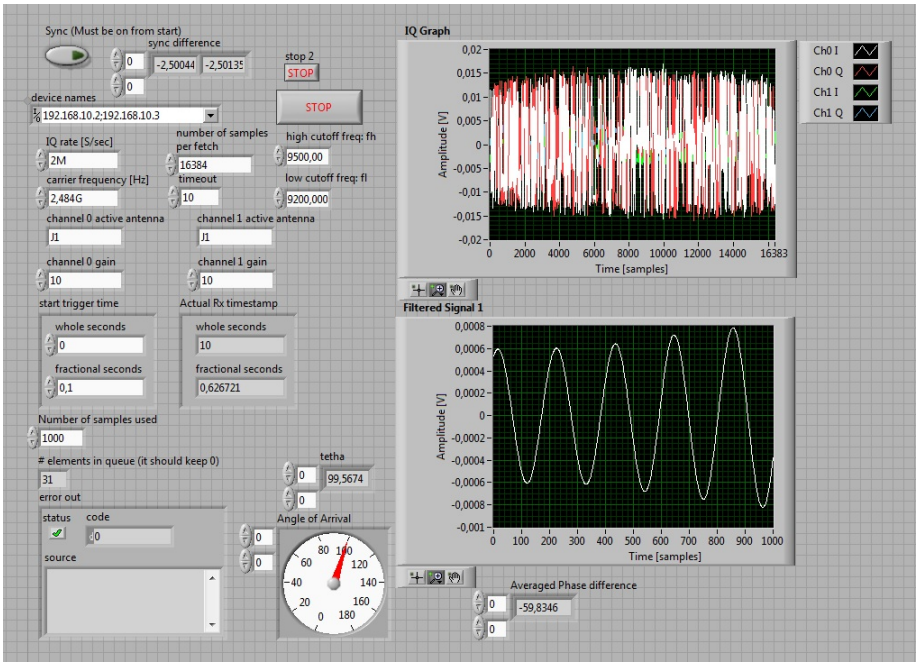

Figure 5.11: Front panel of the finished tracking code in LabVIEW. The front panel is the user interface, where inputs can be defined and all the outputs are displayed

5.4.3 Code Verification

The code had to be verified before measuring the DOA accuracy in the anechoic chamber. In order to imitate a moving target, the phase shifter was adjusted. However, the phase shift was not linear at 2.484 GHz. By connecting the phase shifter between port 1 and 2 of the network analyzer, the phase shift of a signal was measured. The actual phase shift was measured for every 10° theoretical phase shift, for correct reference. Afterwards, the phase difference of the sine signals, and the QPSK modulated signals, was measured in LabVIEW with the second test setup.

Table 5.2: Measured phase difference of the signals in degrees

Theoretical phase difference	Actual phase difference Network Analyzer	Measured phase difference QPSK modulated signal	Measured phase difference Sine signal
0°	0°	0°	0°
10°	7.4°	8°	10°
20°	21°	19°	22°
30°	35.7°	33°	33°
40°	49.5°	47°	48°
50°	63°	61°	60°
60°	76.6°	77°	76°
70°	90.6°	95°	95°
80°	106.6°	113°	113°
90°	122.6°	130°	132°
100°	138.9°	148°	149°
110°	154.3°	162°	163°
120°	171.1°	177°	178°
130°	186.6°	192°	191°
140°	201.6°	203°	203°
150°	216.2°	217°	217°
160°	230.4°	232°	239°
170°	244.7°	246°	246°
180°	259.7°	264°	262°
190°	275.6°	282°	282°
200°	292.9°	301°	300°
210°	309.9°	317°	318°
220°	326.4°	334°	333°
230°	343.7°	347°	348°
240°	359.1°	361°	362°

Table 5.2 shows the phase differences measured in LabVIEW, compared to the reference phase difference measured by the network analyzer. It is evident from the table that the code works at it should, with just small offsets in phase compared to the actual phase difference. Figure 5.12 displays the offsets better, as errors in phase of the actual phase difference. The largest phase error is about 10°, which corresponds to an angle of arrival error of approximately 2°. The requirement for the tracking code is that its accuracy should be within 10% of the receiving antenna's beamwidth. The main receiver antenna have a beamwidth of 20°, so a tracking error of 2° is acceptable.

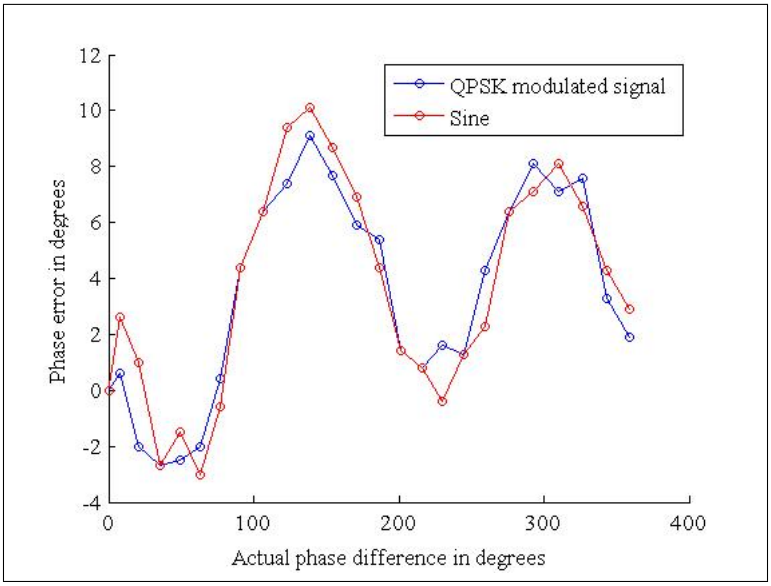

Figure 5.12: The phase error of the phase difference to the measured signals compared to the actual phase difference. The measured signals are a sine generated by the signal generator and a QPSK modulated signal generated in LabVIEW. The actual phase difference is measured by a network analyzer

Chapter 6

Tracking System Measurements

This chapter covers the verification and measurements of the tracking system when the signal is transmitted and received by antennas in an anechoic chamber.

6.1 Measurement Setup

All the measurements in this chapter were taken in an anechoic chamber at NTNU Gløshaugen. An anechoic chamber is a room designed to absorb reflections from sound and electromagnetic waves. It is also insulated from exterior sources of noise. Figure 6.1 shows the anechoic chamber used in this thesis.

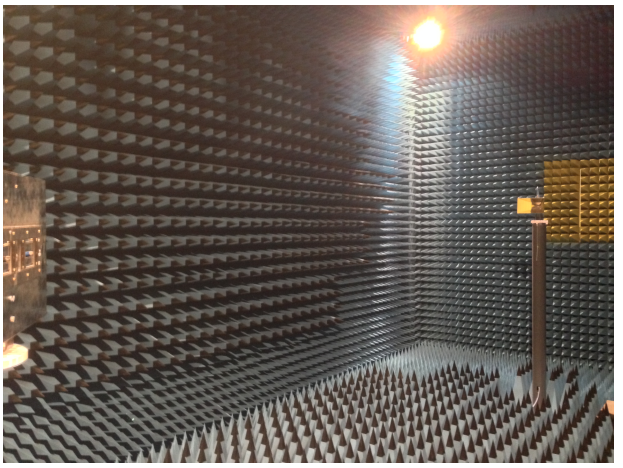

Figure 6.1: The anechoic chamber where the measurements were taken. The transmitter antenna is to the right and the receiver antennas is to the left in the picture.

As mentioned in Chapter 4.1, the two tracking antennas [16] have 9 dB gain, 60° half power beamwidth in the H-plane, and 76° half power beamwidth in the E-plane. The DOA measurements were restricted to ± 30° around 90° angle of arrival, to make sure that the transmitter was within the radiation pattern of the tracking antennas. Otherwise, the antennas wouldl not be able to detect the signal from the transmitter. The tracking antennas were placed as close to each other as possible, because of their physical size. They were separated by a distance of 12 cm between the center of the antennas. With a carrier frequency of 2.484 GHz, 12 cm corresponds to approximately one wavelength. As explained in Chapter 3, a separation distance of a wavelength or more can cause phase detection ambiguities. However, the phase ambiguities occurs at an angle of arrival around 0° or 180° when the separation distance equals a wavelength. Since the DOA measurements were restricted to 60-120°, no phase detection ambiguities should have occured. The receiver antennas were stationed 2.4 meter above the ground, on top of a rotating platform, as shown in Figure 6.2a.

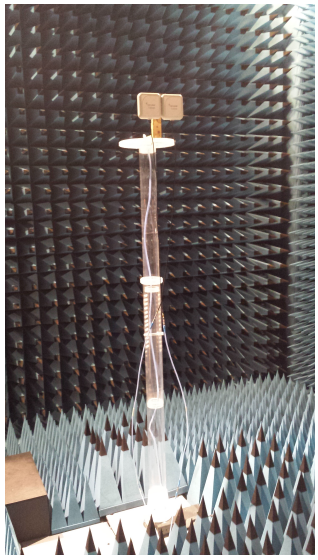

(a) •

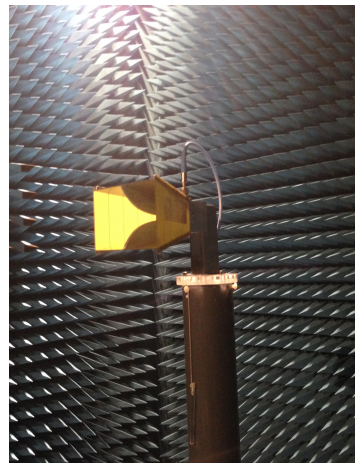

(b) •

Figure 6.2: a) Receiver antennas setup. The two antennas are placed 2.4 meter above the ground, on top of the rotating platform controlled by the motion controller. **b)** 6 dB horn antenna transmitting the QPSK modulated signal directly towards the receiving antennas. It is stationed 2.4 meter above the ground.

The antenna used for transmitting the QPSK modulated signal in the anechoic chamber was an EMCO Model 3115 horn antenna [25]. The horn antenna had approximately 9 dB gain at 2.484 GHz frequency, and was stationed 2.4 meter above the ground. Its radiation pattern was directed towards the receiving antennas. Figure 6.2b displays the horn antenna in the anechoic chamber. The transmitter antenna and the tracking antennas were separated

by a distance of five meters, and each antenna was connected to a USRP2 inside the anechoic chamber by a 2 meter long Sucoflex 104P [23] coaxial cable. At the receiver side, the two USRPs were connected by a MIMO cable, as shown in Figure 6.3. The received signals were fed through a GB Ethernet cable to a host computer outside the chamber. On the transmitter side, the USRP was connected by a GB Ethernet cable to another computer that was generating the QPSK modulated signal, which also was outside the chamber.

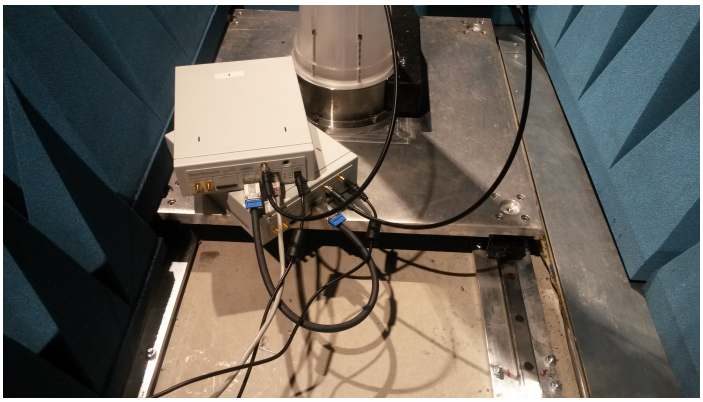

Figure 6.3: System setup, the two USRPs connected to the receiver antennas in the anechoic chamber.

To measure the direction of arrival (DOA) from different directions, the platform with the receiving antennas was rotated by the motion controller displayed in Figure 6.4.

Figure 6.4: Motion controller rotating the platform with the receiver antennas.

There were no reflections or noise interferences in the anechoic chamber. The signal propagated as in free space, thus suffering from free space path loss [4, p.107-108]. In order to have something to compare the measurements with, a theoretical link budget has

been developed for the radio link, based on the measurement setup derived in this chapter. The link budget is shown in Table 6.1. Although the RF daughter board in the USRP has a theoretical maximum output power of 100 mW, the budget uses a transmitted power of 120 mW. The reason why is explained in Chapter 6.2.

Table 6.1: Link budget for tracking antennas in the anechoic chamber

Link Budget	**Input**	**In dB**
Transmitter:		
Transmit power	0.12 W	-9.2 dBW
Antenna gain		9 dBi
EIRP		**-1 dBW**
Propagation:		
Carrier frequency	2.484 GHz	
Distance	5 m	
Free space loss		54.3
Total propagation loss		**54.3**
Receiver:		
Antenna gain		9 dBi
Received power		-15.5 dBm
Cable loss		0.8
Equivalent cable noise temp	58.7 K	
Antenna temp seen from receiver terminals	173.6 K	
Receiver noise figure		5
Equivalent receiver temp	627.1 K	
Receiver system effective noise temp	859.3 K	
Receiver noise in BW		-149.3
C/N		**103.7**
Specifications:		
Receiver sensitivty limit		-105 dBm
Receiver noise N_r		-150.6
System noise N_{sys}		-149.3
Change in sensitivity due to change in noise		1.4
System sensitivity limit		-103.6 dBm
Link Margin		**88.1**

6.2 Measurements and Results

According to the datasheet of the RF daughter board [19], the maximum output power is 100 mW. To make sure the datasheet was correct, the effective transmitted power was measured at the antenna terminals with a spectrum analyzer. With the maximum output settings applied in LabVIEW, the power was measured as 20.8 dBm, which corresponds to approximately 120 mW. Thus, the RF daughter board was able to transmit 20% more power than accounted for in the datasheet. The measured power spectrum is displayed in Figure 6.5, where Ch Pwr corresponds to the total power within the bandwidth, marked by the green lines. With the same settings applied when receiving, the received power was measured at the receiver USRP terminals. Figure 6.6 shows the power spectrum of the received signal, where the received power was measured as -16 dBm.

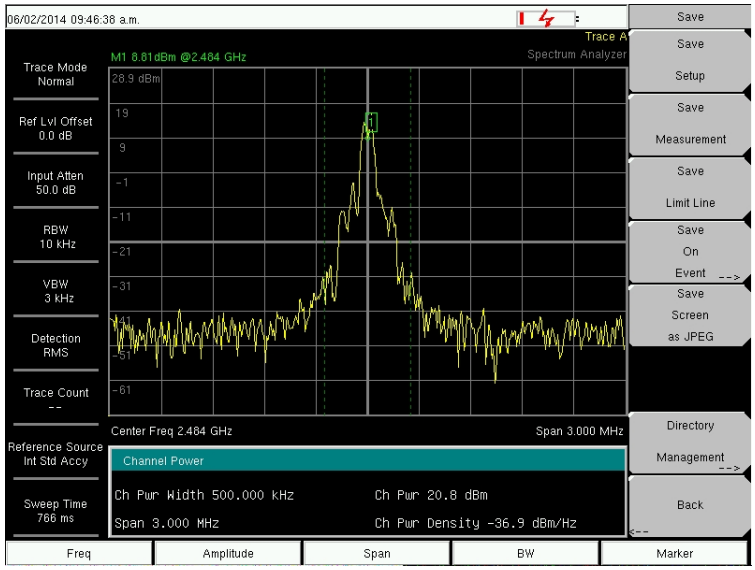

Figure 6.5: Power spectrum of the effective transmitted power at the antenna terminals. The power settings are set to maximum, corresponding to a theoretical output power of 100 mW. The measured output power is 120 mW

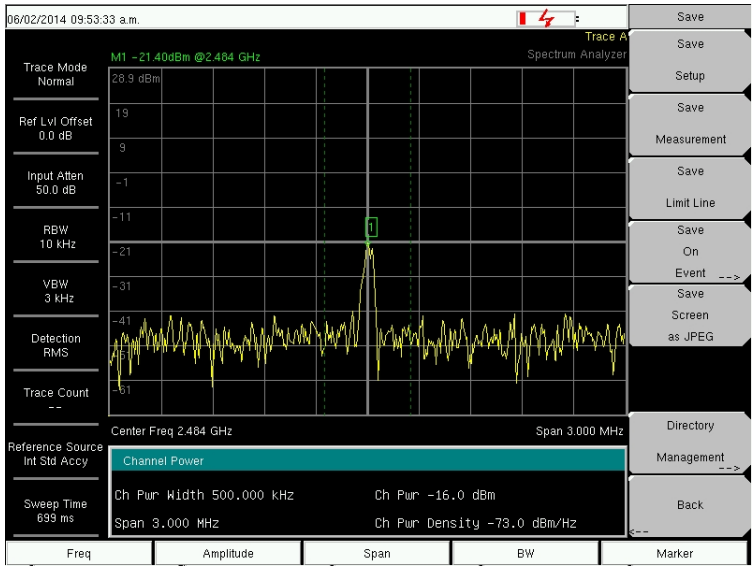

Figure 6.6: Power spectrum of the received signal at the USRP terminals. With 20.8 dBm transmitted power, the received power was measured as -16 dBm.

In order to test the accuracy of the tracking code, the receiver antennas were rotated from 90° to 120°, and from 90° to 60°. The estimated direction of arrival (DOA) was visually read from the code's user interface for every 5°. In addition, the effective transmitted power was varied with different levels of received power in order to test the performance of the code, and to find the minimum power required for a functional code. Table 6.2 displays the measured DOAs for -16 dBm, -36.7 dBm, -45.9 dBm, -56 dBm and -60 dBm received power.

Table 6.2: Measured DOA of the signals in degrees as a function of received power at the USRP terminals.

Actual value	**-16 dBm**	**-36.7 dBm**	**-45.9 dBm**	**-56 dBm**	**-60 dBm**
60°	58.8°	58.5°	58.3°	60°-66°	48°-73°
65°	63.9°	63.4°	63.4°	63°-67°	60°-90°
70°	69°	68.6°	68.7°	67°-72°	60°-80°
75°	74.3°	74°	73.9°	73°-78°	69°-83°
80°	79.6°	79.5°	79.2°	79°-82°	68°-92°
85°	85°	84.8°	84.6°	84°-87°	78°-92°
90°	90.2°	90°	89.8°	87°-95°	84.8°-95.2°
95°	95.5°	95.4°	95.4°	93°-98°	89°-101°
100°	100.9°	100.6°	100.8°	99°-101°	92°-105°
105°	106.2°	106°	106.2°	103°-108°	95°-110°
110°	111.8°	111.5°	111.4°	110°-113°	96°-120°
115°	117.1°	117.1°	117°	113°-120°	109°-124°
120°	122°	122°	122°	122°-127°	113°-131°

The difference between the actual and estimated DOA, or DOA error, describes the accuracy of the tracking system. The DOA errors of the signals with -16 dBm, -36.7 dBm and -45.9 dBm received power from Table 6.2 are plotted in Figure 6.7. Around 90° angle of arrival, the DOA error is close to zero for all three signals, which means that the estimation is nearly 100% accurate. However, the error increases towards the edges, where the error is as large as 2° at 120° angle of arrival, and 1.2° to 1.7° at 60° angle of arrival. The error of the signals are nearly identical for -36.7 dBm and -45.9 dBm received power. The strongest signal, with a received power of -16 dBm, differs slightly from the other two. It has a better accuracy from 90° to 60°, but has a marginally worse accuracy from 90° to 120°.

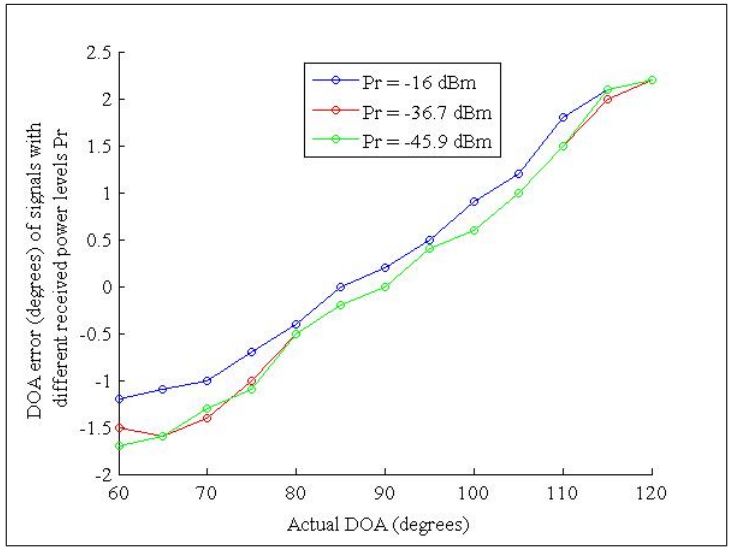

Figure 6.7: The difference between the measured direction of arrivals (DOA) and the actual DOA of QPSK modulated signals with different received powers.

It is not very surprising that the errors are nearly equal, since the budgeted signal-to-noise ratios (SNR), shown in Table 8.4, are very large for these signals. The errors in phase measurements due to the noise are minimal for high SNRs according to Forssell [9, p.70]. By inserting the SNR values from Table 8.4 into Equation (2.24), the theoretical DOA errors due to noise are $9.189 * (10^{-5})$ °, $0.001031°$ and $0,002906°$ for -16 dBm, -36.7 dBm and -45.9 dBm received power respectively. Thus, the error difference between -16 dBm and -36.7 dBm should be insignificant.

Since a change in signal power from -16 dBm to -36.7 dBm did not give a significant reduction in accuracy, then a change in signal power from -16 dBm to -19 dBm should not matter. It is therefore curious that the DOA error increases towards the edges. One possible reason might be because of errors in the calibration. As described in Chapter 5.4.2, the calibration code that synchronizes the phase of the received signals assumes that the sig-

nals are detected from exactly 90° angle of arrival. In the anechoic chamber, the receiver antennas were adjusted towards the transmitter antenna by visual estimation. Therefore, it is highly probable that the code was calibrated to an angle slightly different than 90°. This might cause larger estimation errors at angles that differs greatly from the reference angle, than at angles that are closer to it. An offset in the calibration might also explain why the -16 dBm signal was slightly different than the -36.7 dBm and -45.9 dBm signals, as they might have been calibrated to two different reference angles.

Since the accuracy of DOA estimation is nearly equal for -16, -36.7 and -45.9 dBm received power, it can be concluded that it does not improve much with increased power. However, the DOA errors increases when the power of the received signal reaches a lower limit. As shown in Figure 6.8a and 6.8b, the accuracy of the DOA estimation decreased rapidly from -56 dBm to -60 dBm received power. The estimated DOA for -56 dBm and -60 dBm, from Table 6.2, are plotted as red lines that indicates the boundaries of the varying DOA estimation. In comparison, the ideal estimation is plotted as the blue line. Even though the accuracy of the estimation decreased, the DOA code was still able to estimate the general direction of the transmitter.

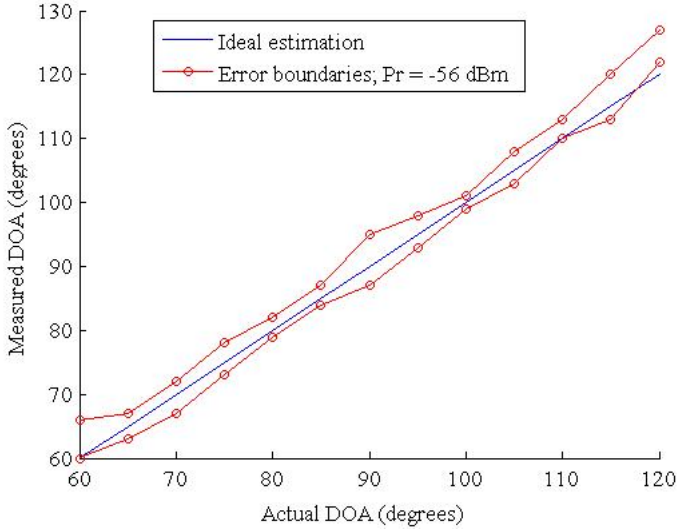

(a) •

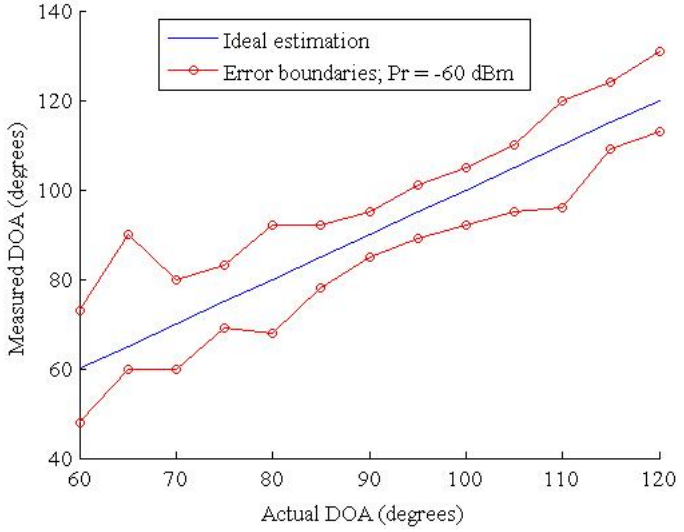

(b) •

Figure 6.8: Measured DOA of a QPSK modulated signal with a received power of **a)** -56 dBm, **b)** -60 dBm. The red lines are the boundaries of the unstable measured DOA, and the blue line is the ideal DOA.

In Figure 6.9a and 6.9b, the DOA estimation errors are plotted for the signals with -56 dBm and -60 dBm received power. In comparison, the errors of -16 dBm and -36.7 dBm received power have also been plotted. The blue lines indicates the boundaries of the unstable error. Comparing Figure 6.9a and 6.9b, it is evident that the error increases substantially by reducing the received power below -56 dBm. At -56 dBm received power, the maximum measured DOA error was 7° at 120° angle of arrival, while at -60 dBm received power the maximum measured DOA error was 25° at 65° angle of arrival. The increase in error is somewhat surprising for these signals, since their SNRs are relatively large. By inserting the SNR values from Table 8.4 into Equation (2.24), the theoretical errors due to noise are $0,009189°$ and $0,01456°$. In other words, the power levels of the signals should be high enough to have close to ideal accuracy. Judging from Figure 6.9a and 6.9b, the errors did not follow the same pattern as the errors of the stronger signals. The error boundaries were more or less random around zero for all the angle of arrivals, while for the stronger signals the error went from negative to positive from 60° to 120°. Since the errors were seemingly random at all angles of arrival, error in calibration was probably not the issue.

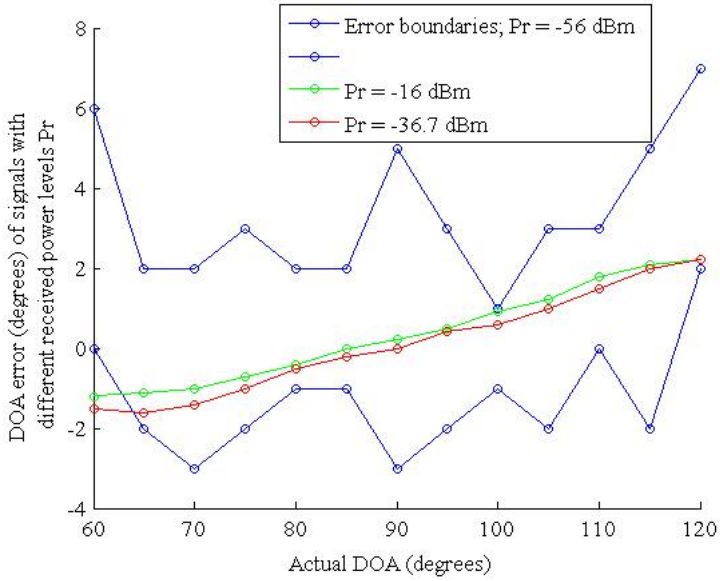

(a) •

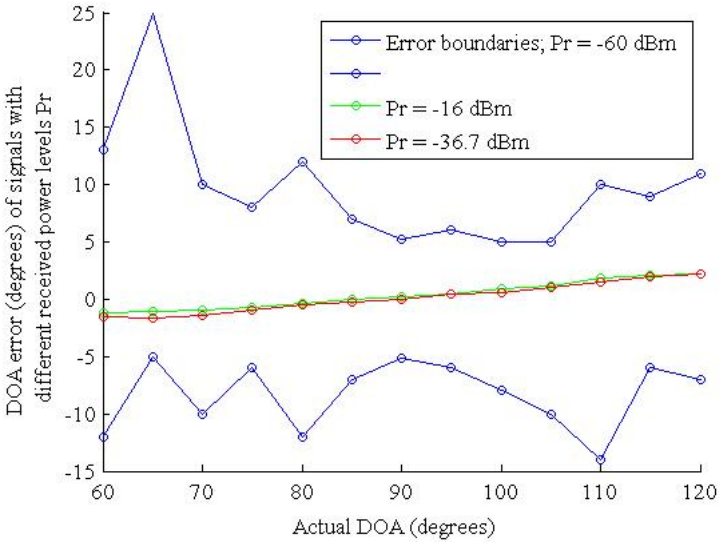

(b) •

Figure 6.9: The difference of the measured direction of arrivals (DOA) compared to the actual DOA of QPSK modulated signals with different received power. The blue lines are the boundaries of the unstable DOA error to the signals with **a)** -56 dBm, **b)** -60 dBm received power.

To ensure optimal radio link between the receiver and the transmitter, the DOA error should not be larger than 10% of the half power beamwidth to the main receiver antenna. The half power beamwidth of the main receiver antenna is 20°, which allows a maximum error of 2°. Seen from Figure 6.7, the DOA errors of the QPSK modulated signals with -16 dBm, -36.7 dBm and -45.9 dBm received power were within the maximum error limit. However, with a received power of -56 dBm and -60 dBm, the accuracy was not sufficient. At -56 dBm received power, the errors were between 2° and 7°, which means that the estimations were still within the half power beamwidth of the main receiver antenna. At -60 dBm received power, the errors were at worst 25°, which is not even within the half power beamwidth. Although the estimation accuracy at -56 dBm received power did not fulfill the error requirement, it was still within the half power bandwidth of the main antenna. Therefore, it is assumed that -56 dBm received power is the lowest power limit of a functional DOA code. The power spectrum of the received signal at -56 dBm power is displayed in Figure 6.10

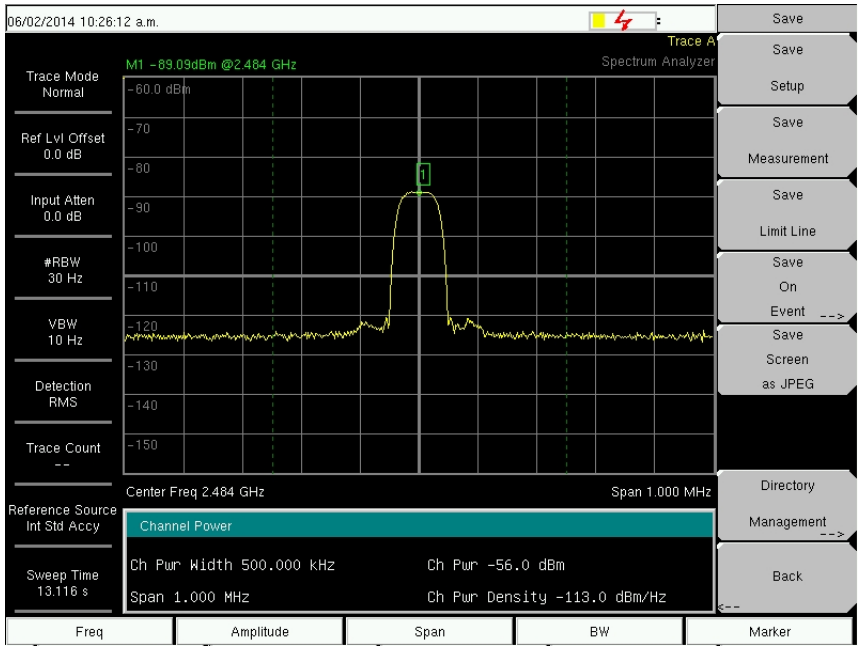

Figure 6.10: Power spectrum of the received signal at the USRP terminals, where the received power is -56 dBm.

The maximum output power of the USRPs was measured as 120 mW, which corresponds to a budgeted received power of -15.5 dBm as shown in Table 6.1. With 120 mW output power in the anechoic chamber, the received power was measured as -16 dBm, which is only 0.5 dB off the budgeted value. By decreasing the received power to -56 dBm in the link budget, the range of the radio link in the anechoic chamber has been estimated as 525 meters. However, this estimation is based on the free space path loss [4, p.107-

108] in the anechoic chamber, and the transmitted power was only 120 mW. In the real communication system, the transmitted power is 1 W and the transmitter antenna gain is 2 dBi instead of 9 dBi. Thus, by using the same received power in the link budget with an increase in transmitted power and transmitter antenna gain, the maximum range of the system is 680 meters in reflection- and interference free conditions. The link budget with the new values can be found in Table 8.2 in the appendix.

Chapter 7

Discussion

Chapter 6 presented and analyzed the results of the measurements done in the anechoic chamber. In order to achieve a good radio link between the unmanned aerial vehicle (UAV) and the ground station, the direction of arrival (DOA) error should not exceed 10% of the half power beamwidth to the main receiver antenna. The half power beamwidth is 20°, allowing a maximum DOA error of 2°. It was found that the accuracy of the DOA code for QPSK modulated signals with a received power from -45.9 dBm fulfills that requirement, since the maximum error was approximately 2° as shown in Figure 6.7. However, this error does not correspond with the theoretical error due to noise, which is approximately zero for these signals. The accuracy, presented as the DOA errors in Figure 6.7 seems to be following a pattern. The errors were large at 60° angle of incidence, decreased towards 90° angle of arrival, then increased again towards 120° angle of arrival where the errors were at their largest. As the errors were nearly equal and followed almost the exact same pattern for different levels of received power, the deviation was probably a systematic error. One of the possible reasons for this systematic error could be an offset in the calibration, which is done assuming the signal arrives from 90° angle of incidence. An offset in the calibration can lead to phase errors in the calculations, that are more noticeable at the edges of the tracking area.

For signals at -56 dBm received power, the accuracy of the system decreased, producing DOA errors between 2° and 7°. Although the estimated DOA was still within the half power beamwidth of the main receiver antenna, the accuracy decreased rapidly as the received power decreased from -56 dBm, as shown in Figure 6.9b. As with the other signal powers, the actual DOA error was much bigger than the theoretical error due to noise. At -56 dBm received power, the budgeted SNR is 63.3 dB, which corresponds to a theoretical error of $0,009189°$. In addition, the error is random, with different values at all angle of arrivals. Unlike the stronger signals, it does not seem like errors in calibration is the cause of the errors, since calibration errors leads to good accuracy around the reference angle, then decreases the further away the angle is to the reference angle. Even if the signal at -56 dBm received power did not fulfill the error requirement, the accuracy of the code was still

good enough to estimate the general direction of the transmitter. Therefore it is prudent to require a minimum received power of -56 dBm for a functional tracking algorithm.

A link budget of the radio link in the anechoic chamber is shown in Table 6.1. It budgets -15.5 dBm received power when the transmitted power is 120 mW. In comparison, the received power was measured as -16 dBm with 120 mW transmitted power, which is a close approximation to the budgeted value. Therefore, the link budget is considered a good model of the actual radio link, and can be used to measure the maximum range. In order to achieve a theoretical range of the system, certain parameters have to be changed in the budget to fit the actual specifications. Changing the transmitted power to 1 W, the received power to -56 dBm, and the transmitter antenna gain to 2 dBi, the range is calculated as 680 m. Thus, the maximum range of the functional tracking system is approximately 680 m in a reflection and interference free environment.

However, under the conditions at Andøya Rocket Range (ARR), where the UAV is flying above the ocean, loss in received power due to reflections is a huge issue, as discussed in Chapter 4.2. If the reflections from the ocean interferes with the direct signal, the propagation loss increases, shown in Figure 4.6 as troughs. When the received power is below -56 dBm due to propagation loss, the accuracy of the DOA estimation is poor, causing the tracking antennas to loose track of the UAV. If the UAV is within the half power beamwidths of the tracking antennas when the propagation loss decreases, the tracking system will be able to track it correctly again. However, information packages might be lost when the system looses track of the UAV. In the worst case scenario, the system will not be able to pick up the correct DOA again, thereby having completely lost track of the UAV. Thus, the maximum range of the tracking system is less than 680 m in reality.

One solution to avoid the loss of signal power due to reflections, is to use a technique called space diversity [6, p.393]. This technique exploits the use of several independent receiving elements with different interference characteristics, to select the best signal at any given time. For instance, by stationing a set of tracking antennas six meters above the ground, in addition to the antennas stationed ten meters above the ground, the signals will have different plane earth path loss characteristics as shown in Figure 7.1. It can be seen from the figure that at some locations where one signal suffers a huge drop in signal strength, the other signal have a peak. Thus, by selecting the best signal at any given time, most of the loss due to reflections can be avoided.

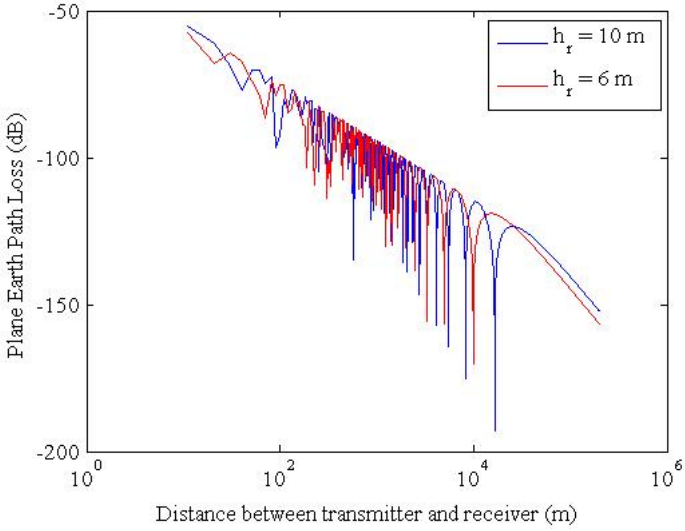

Figure 7.1: Overlapping plane earth path loss at receiver antennas stationed 6 m and 10 m above the ground. The transmitter antenna is stationed 100 m above the ground

The goal was to design a tracking system with a range of 20 km. At best, by using antenna diversity, the designed tracking system has a maximum range of 680 meters, which is 19320 meters off the requirement. One way to achieve the desired range is to increase the receiver antenna gain from 9 dBi to 38.4 dBi. It can be done by using a huge antenna array. However, the goal was to create this system with only two antennas, so the antennas have to be more directive instead. An increase in directivity leads to an increase in physical size. Antennas with 38.4 dBi gain are very large, causing the separation distance between the centers of the antennas to be larger than a wavelength. Hence, an increase in antenna gain leads to a phase detection ambiguity in the DOA code, which causes the code to estimate the wrong DOA. It is evident that an increase in antenna gain is not the way to go for this particular tracking code. Also, 9 dBi receiver antenna gain should be sufficient to provide a stable radio link within 20 km according to Table 8.1, given the right precautions. The table shows the link budget to the tracking system in real conditions, where the link margin to the radio link is 21.9 dB at 20 km. It is also apparent from Figure 6.10 that the signal strength of the received signal is above the noise floor with a good margin. Thus, the sensitivity of the receiver is not the problem.

Excluding the receiver and the antennas, the only remaining option is to improve the code. As mentioned in Chapter 5.4.2, the signals are filtrated by a bandpass filter with 300 Hz bandwidth. Figure 6.10 shows that the bandwidth of the received QPSK modulated signal was approximately 100 kHz. The power density of the signal was -113 dBm/Hz, which resulted in -56 dBm received power. In all the calculations, the bandwidth of the received signal was assumed to be 100 kHz. But due to the filters, the actual bandwidth of the system is only 300 Hz. With a power density of -113 dBm/Hz, the received power after

the filtering is -88.2 dBm. This means that if the receiver receives -56 dBm power, the code only utilizes -88.2 dBm power. By using -88.2 dBm received power as the minimum limit in the link budget with 1 W transmitted power and 2 dBi transmitter antenna gain, the calculated maximum range in the anechoic chamber is 27600 meters, assuming all the received power is utilized. The link budget can be found in Table 8.3 in the appendix. The corresponding SNR is 31 dB, which gives a theoretical DOA error of 0.37° due to noise. This still does not quite match the measured DOA error, so it is apparent that something else was influencing the DOA estimation, or that the link budget is wrong. However, It is no doubt that the filters in the code reduces the potential range of the radio link severely.

The tracking code also suffer from other limitations. One of the worst limitations is that the filters are very narrow banded. If the signals suffers Doppler shifts [6, p.228] in the channel, the carrier frequency might be shifted out of the range of the bandpass filter. In effect, the filter would remove the part of the signal that the DOA code needs to function. Another limitation of the code is the way it handles the calibration of the signals. In order to achieve a correct calibration, the transmitter has to be stationed directly at an angle of 90° to the receiver antennas, as mentioned in Chapter 5.4.2. An offset in the calibration leads to DOA errors at angles that are not close to the reference angle.

Since the tracking code did not fulfill all the requirements, and suffers certain limitations, a different method of tracking is more appropriate. As discussed in Chapter 5.3, carrier recovery with a Costas loop [12, p.57], [13, p.229] is a better method for this particular radio link. The Costas loop uses coherent quadrature signals to measure the phase error of the signals without filtering away most of the received signal power. Thus, replacing the filters and phase calculation code with a Costas loop allows for a much larger range. The method is also independent on knowing the carrier frequency of the signal in order to find the phase error, therefore it is proof against Doppler shifts.

Chapter 8

Conclusion

This thesis has presented the design of a tracking algorithm for tracking of an unmanned aerial vehicle at Andøya Rocket Range. The accuracy of the tracking algorithm was tested in an anechoic chamber, for different levels of received power. At -16 dBm, -36.7 dBm, and -45.9 dBm received power, the estimated direction of arrival errors were nearly identical, with a maximum error of 2° at 120° angle of arrival. The maximum error allowed is 10% of the half power beamwidth of the main receiver antenna, which corresponds to 2°. Thus, signals with a received power of -45.9 dBm or higher fulfills the accuracy requirement.

At -56 dBm received power, the estimated direction of arrival error was between 2° to 7°. Although the accuracy requirement is not fulfilled, the estimated direction of arrival was still within the half power beamwidth of the main receiver antenna. Therefore, it is assumed that -56 dBm is the minimum required power in order to have a functional tracking system. Assuming that the transmitter antenna transmits with 1 W power, and that the received power is -56 dBm, the estimated maximum range is 680 meters under reflection- and interference free conditions. Thus, the range requirement of 20 km is not fulfilled.

The reason why the tracking system does not fulfill the range requirement, is because the bandpass filters in the tracking algorithm are very narrow banded. The received signal power is spread out in a frequency band of approximately 100 kHz, with a power density of -113 dBm/Hz. Since the filter is narrow banded, only -88.2 dBm of the -56 dBm received power is actually utilized in the code. Assuming that the code is functional without the filters, the estimated maximum range is 27600 meters under reflection- and interference free conditions. However, the received signal will suffer tremendous loss due to reflections in the tracking system's intended environment. The additional loss leads to a maximum range far below 27600 meters. Thus, to fulfill the range requirement, space diversity should be introduced in the tracking system to reduce the loss due to reflections. In addition, the filter and phase estimation code in the current tracking code should be replaced by a more appropriate phase estimation method, which utilizes all the received

power. One such method is the carrier recovery method with a Costas loop [12, p.57], [13, p.229].

8.1 Recommendations for Further Work

In order to utilize all of the received power, the bandpass filter and the phase estimation code should be replaced with a Costas loop. The Costas loop detects the phase of the two received signals, and retains the received power. The phase difference should then be sent on to the averaging and DOA code. The benefits of using a Costas loop is that the maximum range of the system increases. In addition, the Costas loop works independently of knowing the carrier frequency of the signal, thus a shift in the frequency due to Doppler shift will not affect the phase detection.

By using a Costas loop, the maximum range of the system should be able to fulfill the range requirement under reflection- and interference free conditions. However, since the tracking system is ment to track a UAV flying above ocean, heavy loss in signal power due to reflections is expected. In order to remove the sudden loss in power due to reflections, space diversity should be used. By introducing a new set of tracking antennas above or underneath the other tracking antennas, the receiver will be able to choose from two independent set of signals. These signals are affected by different interference characteristics, as the occurrence of cancellations are dependent on the position of the receiving antennas, as shown in Figure 7.1. Hence, the sudden losses in signal power can be avoided, and the system can fulfill the range requirements.

This thesis has demonstrated the principle of tracking by finding the direction of arrival. In order to finish the prototype, the tracking antennas should be mounted on a rotating platform controlled by a motion controller. The motion controller should receive its inputs from the tracking system, thereby rotating the antennas in the direction of arrival.

The tracking system should be tested for outdoor use, preferably by moving the transmitter above the ocean. To begin with, the DOA estimation should be evaluated at short distances, then compared with the measured values from the anechoic chamber. If the code is working properly, the distance of the radio link should be gradually increased in order to determine the maximum range of the functioning system.

Bibliography

[1] C.A. Balanis. *Antenna Theory: Analysis and Design*. Knovel library. Wiley, 2005.

[2] Datasheet Piccolo 2 Ground Station. `https://www.cloudcaptech.com/Sales%20and%20Marketing%20Documents/Piccolo%20Ground%20Station%20Data%20Sheet.pdf`. Accessed: 13-05-2014.

[3] Datasheet MHS100200 - Spectra-2400 Radio. `https://www.cloudcaptech.com/Download/Piccolo/RF%20Spectrum%20Information/DD-1494%20Spectrum%20Data%20for%20Piccolo%20II%202400%20MHz%20Radio.pdf`. Accessed: 13-05-2014.

[4] T.S. Rappaport. *Wireless communications: principles and practice*. Prentice Hall communications engineering and emerging technologies series. Prentice Hall PTR, 2002.

[5] *Field & Wave Electromagnetics, 2/E*. Pearson Education, 1989.

[6] S. Saunders and A. Aragón-Zavala. *Antennas and Propagation for Wireless Communication Systems: 2nd Edition*. John Wiley & Sons, 2007.

[7] D.M. Pozar. *Microwave and RF Wireless Systems*. Wiley, 2001.

[8] T. Manning. *Microwave Radio Transmission Design Guide*. Artech House Microwave Library. Artech House, Incorporated, 2009.

[9] B. Forssell. *Radionavigation systems*. Prentice Hall, 1991.

[10] J. Foutz, A. Spanias, and M.K. Banavar. *Narrowband Direction of Arrival Estimation for Antenna Arrays*. Synthesis lectures on antennas. Morgan & Claypool Publishers, 2008.

[11] R.O. Schmidt. Multiple emitter location and signal parameter estimation. *Antennas and Propagation, IEEE Transactions on*, 34(3):276–280, Mar 1986.

[12] D.B. Talbot. *Frequency Acquisition Techniques for Phase Locked Loops*. Wiley, 2012.

[13] R. Dixon. *Radio Receiver Design*. Electrical and Computer Engineering. Taylor & Francis, 1998.

[14] Datasheet 18 dBi Receiver Antenna. http://www.wimo.de/download/sp-2g4.pdf. Accessed: 13-05-2014.

[15] 2 dBi Stub Antenna used in the UAV. https://www.elfaelektronikk.no/elfa3~no_en/elfa/init.do?init=2&shop=ELFA_NO-EN&item=73-009-85. Accessed: 13-05-2014.

[16] Datasheet TL-ANT2409A Directive Antenna. http://www.tp-link.com/Resources/document/TL-ANT2409A_V1_Datasheet.zip. Accessed: 19-05-2014.

[17] Datasheet Coaxial Cable - H1000C1. https://www1.elfa.se/data1/wwwroot/assets/datasheets/05591425.pdf. Accessed: 19-05-2014.

[18] USRP2 Datasheet. http://www.olifantasia.com/gnuradio/usrp/files/datasheets/ds_usrp2.pdf. Accessed: 21-05-2014.

[19] USRP2 Daughter Board XCVR2450 Datasheet. http://www.olifantasia.com/gnuradio/usrp/files/datasheets/ds_transceiver.pdf. Accessed: 21-05-2014.

[20] National Instruments LabVIEW, Graphical Programming Language. http://www.ni.com/labview/. Accessed: 21-05-2014.

[21] Pasternack RG 223/U Coaxial Cable Datasheet. http://www.pasternack.com/images/ProductPDF/RG223-U.pdf. Accessed: 21-05-2014.

[22] USRP2 Device Manual. http://files.ettus.com/uhd_docs/manual/html/usrp2.html. Accessed: 09-06-2014.

[23] Huber+Suhner Sucoflex 104P Coaxial Cable Datasheet. http://www2.hubersuhner.com/mozilla/write_product_document?prm=5DF39C616E2B98A3A44E695951995123&file=025953BD6653A2BDAF05AB4A4DB0080A&type=A8F83C4692AC6C94A5DEED64242DB322. Accessed: 19-05-2014.

[24] G.C. Josephson. On the definition and measurement of occupied bandwidth. *Electromagnetic Compatibility, IEEE Transactions on*, EMC-12(2):33–37, May 1970.

[25] Datasheet EMCO Model 3115 Horn Antenna. http://www.atecorp.com/ATECorp/media/pdfs/data-sheets/EMCO-3106-3115-3116_Datasheet.pdf. Accessed: 02-06-2014.

Appendix

Calculations

Plane Earth Path Loss at a Range of 20 km

The theory and formula can be found in Chapter 2.1.3. The specifications are:

Distance between antennas d = 20 km
Frequency f = 2.484 GHz
Wavelength λ = 0.12077 m
Free space wavenumber k = 52.02
Transmitter height above ground h_t = 100 m
Receiver height above ground h_r = 10 m

From (2.11), the plane earth path loss is given as

$$\frac{P_r}{P_t} = 2\left(\frac{\lambda}{4\pi d}\right)^2 \left[1 - cos\left(k\frac{2h_t h_r}{d}\right)\right] = 126.1dB \tag{8.1}$$

System Sensitivity Limit of Main Receiver Antenna

This section presents the calculations of the system sensitivity limit and the terms used to calculate it for the radio link with the 18 dBi reflector antenna as receiver. The theory and formulas can be found in Chapter 2.2.

Reference temperature T_0 = 290 K
LNA gain G_{LNA} = 13 dB
LNA noise figure F_{LNA} = 1.1 dB = 1.29
LNA noise temperature is given by

$$T_{LNA} = (F_{LNA} - 1)T_0 = 83.6K \tag{8.2}$$

Cable length l_{bLNA} before LNA = 0.1 m
Cable loss G_{bLNA} before LNA = 0.023 dB
Cable noise temperature before LNA is given by

$$T_{bLNA} = (10^{\frac{G_{bLNA}}{10}} - 1)T_0 = 1.5K \tag{8.3}$$

Cable length l_{aLNA} after LNA = 10 m
Cable loss G_{aLNA} after LNA = 2.3 dB

Cable noise temperature after LNA is given by

$$T_{aLNA} = (10^{\frac{G_{aLNA}}{10}} - 1)T_0 = 202.5K \tag{8.4}$$

Receiver noise figure F_r = 5 dB
Receiver noise temperature is given by

$$T_r = (10^{\frac{F_r}{10}} - 1)T_0 = 627.1K \tag{8.5}$$

From (2.13), the cascade noise temperature T_{sys} is given by

$$T_{sys} = T_{LNA} + \frac{T_{aLNA}}{G_{LNA}} + \frac{T_r}{G_{LNA}G_{aLNA}} = 147.1K \tag{8.6}$$

Antenna noise temperature seen from the antenna terminals T_A = 150K
Attenuation coefficient α = 0.23 dB/m and is given in Np/m by (2.15)

$$\alpha(Np/m) = \frac{\alpha(dB/m)}{20(log_{10}e)} = 0.026763Np/m \tag{8.7}$$

Transmission line length is given by

$$l = l_{bLNA} + l_{aLNA} = 10.1m \tag{8.8}$$

Thermal efficiency e_A = 100%
Physical antenna temperature T_p = 290 K
Physical antenna temperature seen from the antenna terminals is given by (2.16)

$$T_{AP} = \left(\frac{1}{e_A} - 1\right) T_p = 0K \tag{8.9}$$

From (2.14), the antenna temperature seen from the receiver terminals is given by

$$T_a = T_A e^{-2\alpha l} + T_{AP} e^{-2\alpha l} + T_0(1 - e^{-2\alpha l}) = 208K \tag{8.10}$$

Receiver system effective noise temperature T_{rs} from (2.12) is given by

$$T_{rs} = T_a + T_{bLNA} + T_{sys} = 356.7K \tag{8.11}$$

Boltsmanns constant k = $1.38 * 10^{-23}$
Bandwidth B = 210 kHz
Receiver sensitivity limit SL_r = -105 dBm
Receiver noise is given by

$$N_r = kT_rB = -147.4dB \tag{8.12}$$

System noise is given by (2.19)

$$N_{rs} = kT_{rs}B = -149.9dB \tag{8.13}$$

Thus, from (2.17), the system sensitivity limit is calculated as

$$SL_{sys}(dBm) = SL_r(dBm) + (N_{rs} - N_r)(dB) = SL_r(dBm) + \Delta N(dB) = -107.5dBm \tag{8.14}$$

System Sensitivity Limit of Tracking Antennas in Real Conditions

This section presents the calculations of the system sensitivity limit and the terms used to calculate it for the radio link with the 9 dBi tracking antenna as receiver antenna. The theory and formulas can be found in Chapter 2.2.

Reference temperature T_0 = 290 K
LNA gain G_{LNA} = 13 dB
LNA noise figure F_{LNA} = 1.1 dB = 1.29
LNA noise temperature is given by

$$T_{LNA} = (F_{LNA} - 1)T_0 = 83.6K \tag{8.15}$$

Cable length l_{bLNA} before LNA = 0.1 m
Cable loss G_{bLNA} before LNA = 0.023 dB
Cable noise temperature before LNA is given by

$$T_{bLNA} = (10^{\frac{G_{bLNA}}{10}} - 1)T_0 = 1.5K \tag{8.16}$$

Cable length l_{aLNA} after LNA = 10 m
Cable loss G_{aLNA} after LNA = 2.3 dB
Cable noise temperature after LNA is given by

$$T_{aLNA} = (10^{\frac{G_{aLNA}}{10}} - 1)T_0 = 202.5K \tag{8.17}$$

Receiver noise figure F_r = 5 dB
Receiver noise temperature is given by

$$T_r = (10^{\frac{F_r}{10}} - 1)T_0 = 627.1K \tag{8.18}$$

From (2.13), the cascade noise temperature T_{sys} is given by

$$T_{sys} = T_{LNA} + \frac{T_{aLNA}}{G_{LNA}} + \frac{T_r}{G_{LNA}G_{aLNA}} = 147.1K \tag{8.19}$$

Antenna noise temperature seen from the antenna terminals T_A = 150K
Attenuation coefficient α = 0.23 dB/m and is given in Np/m by (2.15)

$$\alpha(Np/m) = \frac{\alpha(dB/m)}{20(log_{10}e)} = 0.026763Np/m \tag{8.20}$$

Transmission line length is given by

$$l = l_{bLNA} + l_{aLNA} = 10.1m \tag{8.21}$$

Thermal efficiency e_A = 100%
Physical antenna temperature T_p = 290 K
Physical antenna temperature seen from the antenna terminals is given by (2.16)

$$T_{AP} = \left(\frac{1}{e_A} - 1\right) T_p = 0K \tag{8.22}$$

From (2.14), the antenna temperature seen from the receiver terminals is given by

$$T_a = T_A e^{-2\alpha l} + T_{AP} e^{-2\alpha l} + T_0(1 - e^{-2\alpha l}) = 208K \tag{8.23}$$

Receiver system effective noise temperature T_{rs} from (2.12) is given by

$$T_{rs} = T_a + T_{bLNA} + T_{sys} = 356.7K \tag{8.24}$$

Boltsmanns constant k = $1.38 * 10^{-23}$
Bandwidth B = 210 kHz
Receiver sensitivity limit SL_r = -105 dBm
Receiver noise is given by

$$N_r = kT_rB = -147.4dB \tag{8.25}$$

System noise is given by (2.19)

$$N_{rs} = kT_{rs}B = -149.9dB \tag{8.26}$$

Thus, from (2.17), the system sensitivity limit is calculated as

$$SL_{sys}(dBm) = SL_r(dBm) + (N_{rs} - N_r)(dB) = SL_r(dBm) + \Delta N(dB) = -107.5dBm \tag{8.27}$$

System Sensitivity Limit of Tracking Antennas under Reflection and Interference Free Conditions

This section presents the calculations of the system sensitivity limit and the terms used to calculate it for the radio link with the 9 dBi tracking antenna as receiver antenna. The theory and formulas can be found in Chapter 2.2.

Reference temperature T_0 = 290 K
Cable length l = 2 m
Cable loss G_c = 0.8 dB
Cable noise temperature is given by

$$T_c = (10^{\frac{G_c}{10}} - 1)T_0 = 58.7K \tag{8.28}$$

Receiver noise figure F_r = 5 dB
Receiver noise temperature is given by

$$T_r = (10^{\frac{F_r}{10}} - 1)T_0 = 627.1K \tag{8.29}$$

Antenna noise temperature seen from the antenna terminals T_A = 150K
Attenuation coefficient α = 0.4 dB/m and is given in Np/m by (2.15)

$$\alpha(Np/m) = \frac{\alpha(dB/m)}{20(log_{10}e)} = 0.046083Np/m \tag{8.30}$$

Thermal efficiency e_A = 100%

Physical antenna temperature T_p = 290 K

Physical antenna temperature seen from the antenna terminals is given by (2.16)

$$T_{AP} = \left(\frac{1}{e_A} - 1\right) T_p = 0K \tag{8.31}$$

From (2.14), the antenna temperature seen from the receiver terminals is given by

$$T_a = T_A e^{-2\alpha l} + T_{AP} e^{-2\alpha l} + T_0(1 - e^{-2\alpha l}) = 173.6K \tag{8.32}$$

Receiver system effective noise temperature T_{rs} from (2.12) is given by

$$T_{rs} = T_c + T_a + T_r = 859.3K \tag{8.33}$$

Boltsmanns constant k = $1.38 * 10^{-23}$

Bandwidth B = 100 kHz

Receiver sensitivity limit SL_r = -105 dBm

Receiver noise is given by

$$N_r = kT_rB = -150.6dB \tag{8.34}$$

System noise is given by (2.19)

$$N_{rs} = kT_{rs}B = -149.3dB \tag{8.35}$$

Thus, from (2.17), the system sensitivity limit is calculated as

$$SL_{sys}(dBm) = SL_r(dBm) + (N_{rs} - N_r)(dB) = SL_r(dBm) + \Delta N(dB) = -103.6dBm \tag{8.36}$$

Figures and Code

Link Budget of the Radio Link with the Tracking Antennas in Real Conditions, with 1 W Transmitted Power

Table 8.1: Link budget for tracking antennas in real conditions, with 1 W transmitted power

Link Budget	**Input**	**In dB**
Transmitter:		
Transmit power	1 W	0 dBW
Antenna gain		2 dBi
EIRP		**2 dBW**
Propagation:		
Carrier frequency	2.484 GHz	
Distance	20 km	
Plane earth path loss		126.1
Polarization loss		0.5
Total propagation loss		**126.6**
Receiver:		
Antenna gain		9 dBi
Received power		-85.6 dBm
LNA gain		13
LNA noise figure		1.1
LNA noise temp	83.6 K	
Cable loss before LNA		0.0
Equivalent cable noise temp before LNA	1.5 K	
Cable loss after LNA		2.3
Equivalent cable noise temp after LNA	202.5 K	
Antenna temp seen from receiver terminals	208 K	
Receiver noise figure		5
Equivalent receiver temp	627.1 K	
System noise temp	147.1 K	
Receiver system effective noise temp	356.7 K	
Receiver noise in BW		-149.9
C/N		**34.3**
Specifications:		
Receiver sensitivty limit		-105 dBm
Receiver noise N_r		-147.4
System noise N_{sys}		-149.9
Change in sensitivity due to change in noise		-2.5
System sensitivity limit		-107.5 dBm
Link Margin		**21.9**

Link Budget of the Radio Link with the Tracking Antennas in Reflection- and Interference Free Conditions, with 1 W Transmitted Power

Table 8.2: Link budget for tracking antennas in reflection- and interference free conditions, with 1 W transmitted power

Link Budget	**Input**	**In dB**
Transmitter:		
Transmit power	1 W	0 dBW
Antenna gain		2 dBi
EIRP		**2 dBW**
Propagation:		
Carrier frequency	2.484 GHz	
Distance	680 m	
Plane earth path loss		97.0
Total propagation loss		**97.0**
Receiver:		
Antenna gain		9 dBi
Received power		-56 dBm
Cable loss		0.8
Equivalent cable noise temp	58.7 K	
Antenna temp seen from receiver terminals	173.6 K	
Receiver noise figure		5
Equivalent receiver temp	627.1 K	
System noise temp	627.1 K	
Receiver system effective noise temp	859.3 K	
Receiver noise in BW		-149.9
C/N		**63.3**
Specifications:		
Receiver sensitivty limit		-105 dBm
Receiver noise N_r		-150.6
System noise N_{sys}		-149.3
Change in sensitivity due to change in noise		1.4
System sensitivity limit		-103.6 dBm
Link Margin		**47.6**

New Link Budget of the Radio Link with the Tracking Antennas in Reflection- and Interference Free Conditions, with 1 W Transmitted Power

Table 8.3: New link budget for tracking antennas in reflection- and interference free conditions, with 1 W transmitted power

Link Budget	**Input**	**In dB**
Transmitter:		
Transmit power	1 W	0 dBW
Antenna gain		2 dBi
EIRP		**2 dBW**
Propagation:		
Carrier frequency	2.484 GHz	
Distance	27600 m	
Plane earth path loss		129.2
Total propagation loss		**129.2**
Receiver:		
Antenna gain		9 dBi
Received power		-88.2 dBm
Cable loss		0.8
Equivalent cable noise temp	58.7 K	
Antenna temp seen from receiver terminals	173.6 K	
Receiver noise figure		5
Equivalent receiver temp	627.1 K	
System noise temp	627.1 K	
Receiver system effective noise temp	859.3 K	
Receiver noise in BW		-149.9
C/N		**31.1**
Specifications:		
Receiver sensitivty limit		-105 dBm
Receiver noise N_r		-150.6
System noise N_{sys}		-149.3
Change in sensitivity due to change in noise		1.4
System sensitivity limit		-103.6 dBm
Link Margin		**15.5**

Calculated Signal-to-Noise Ratios for Signals with -16 dBm, -37.6 dBm, -45.9 dBm, -56 dBm and -60 dBm Received Power in the Anechoic Chamber

Table 8.4: SNR calculations for signals with different received power.

Received Power	-16 dBm	-36.7 dBm	-45.9 dBm	-56 dBm	-60 dBm
Cable loss	0.8 dB	0.8 dB	0.8 dB	0.8 dB	0.8 dB
Cable noise temp	58.7 K	58.7 K	58.7 K	58.7 K	58.7 K
Antenna temp at USRP terminal	173.6 K	173.6 K	173.6 K	173.6 K	173.6 K
USRP noise figure	5 dB	5 dB	5 dB	5 dB	5 dB
Receiver noise temp	627.1 K	627.1 K	627.1 K	627.1 K	627.1 K
System effective noise temp	859.3 K	859.3 K	859.3 K	859.3 K	859.3 K
Receiver noise in BW	-149.3 dB	-149.3 dB	-149.3 dB	-149.3 dB	-149.3 dB
SNR	103.3 dB	82.6 dB	73.4 dB	63.3 dB	59.3 dB

MATLAB Code for Clearance of Fresnel Zone

```
close all
clear all

d = 0:100:20000;
c = 3*10^8;
f = 2.4*10^9;
lambda = c/f;
distance = 20000;
k = 4/3;
L1 = 10;
L2 = 100;
step = (L2-L1)/distance;

for n = 1:length(d)
    HOFG(n) = L1 + step*d(n);  %HOFG = Height Over Flat Ground
    d2(n) = distance - d(n);
    F(n) = sqrt(lambda*d(n)*d2(n)/(d(n) + d2(n))); %First fresnel zone
    F60(n) = F(n);  % 60% coverage of first fresnel zone
    h(n) = ((d(n)/1000)*(d2(n)/1000))/(12.75*k);
    Clearance(n) = HOFG(n) - F60(n) - h(n);
end

plot(d, Clearance)
xlabel('Distance between antennas (meters)')
ylabel('Clearance for 100% coverage of 1st FZ (meters)')
```

LabVIEW VI of niUSRP EX Rx Multiple Synchronized Inputs

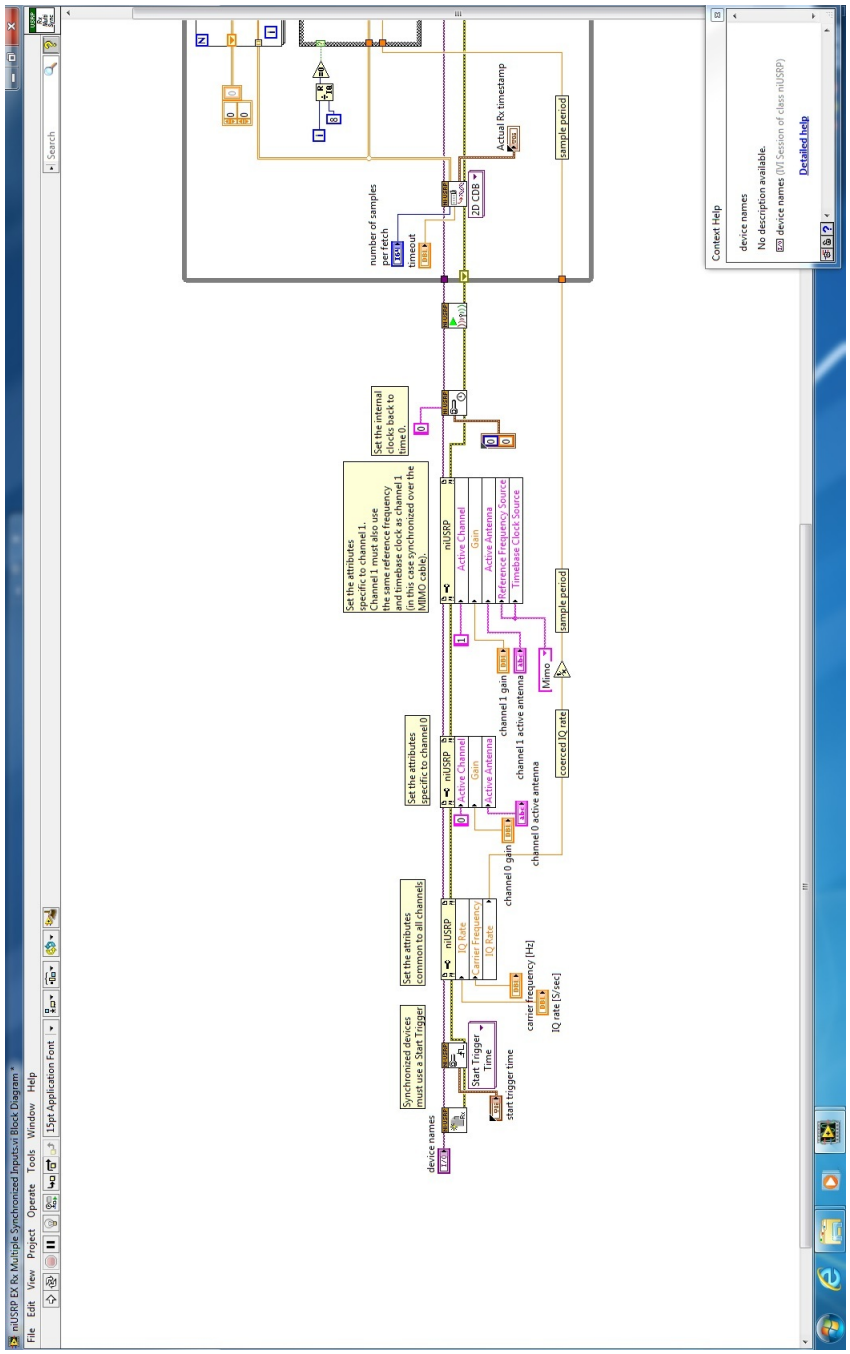

Figure 8.1: Complete VI of niUSRP EX Rx Multiple Synchronized Inputs part 1

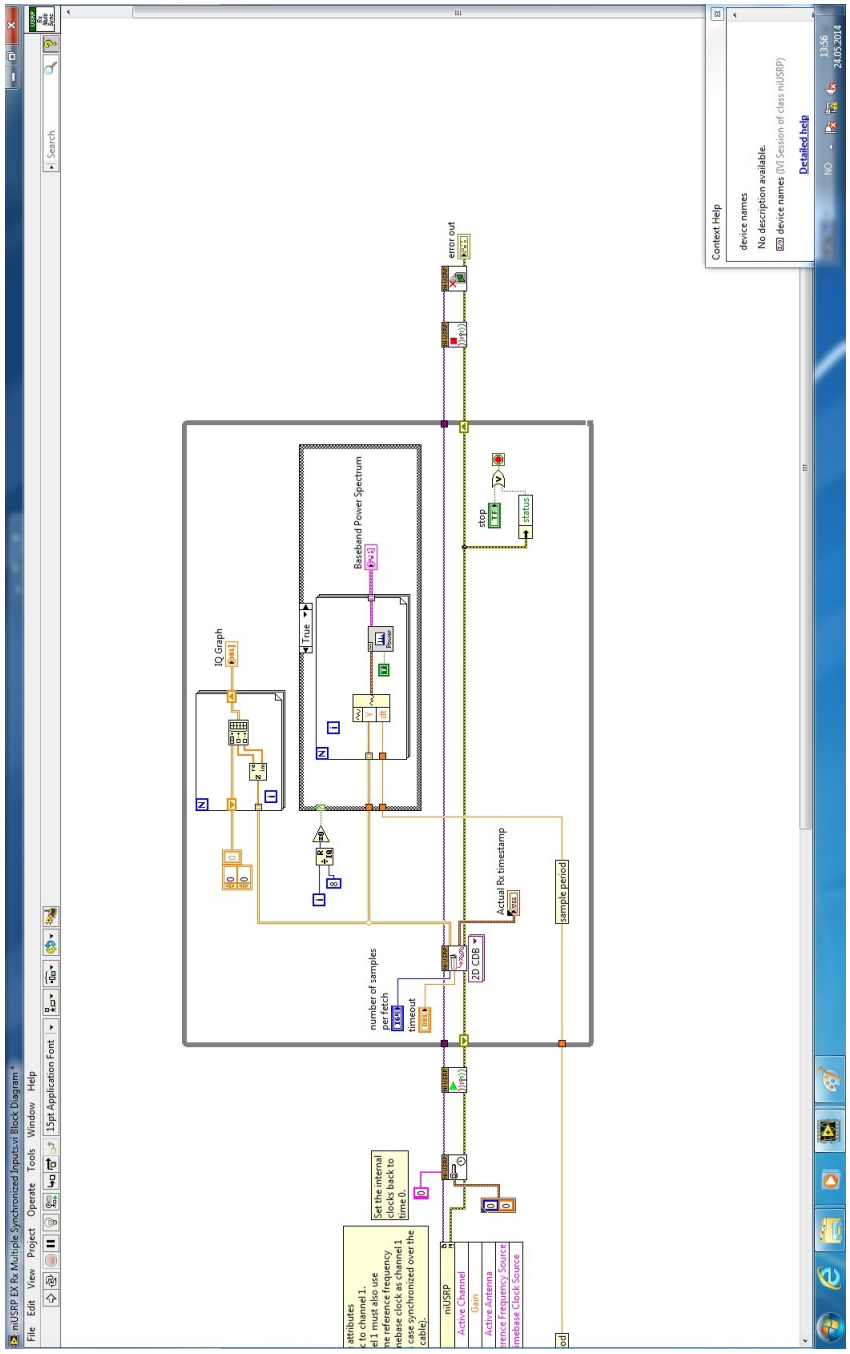

Figure 8.2: Complete VI of niUSRP EX Rx Multiple Synchronized Inputs part 2

LabVIEW VI of Finished Tracking Code

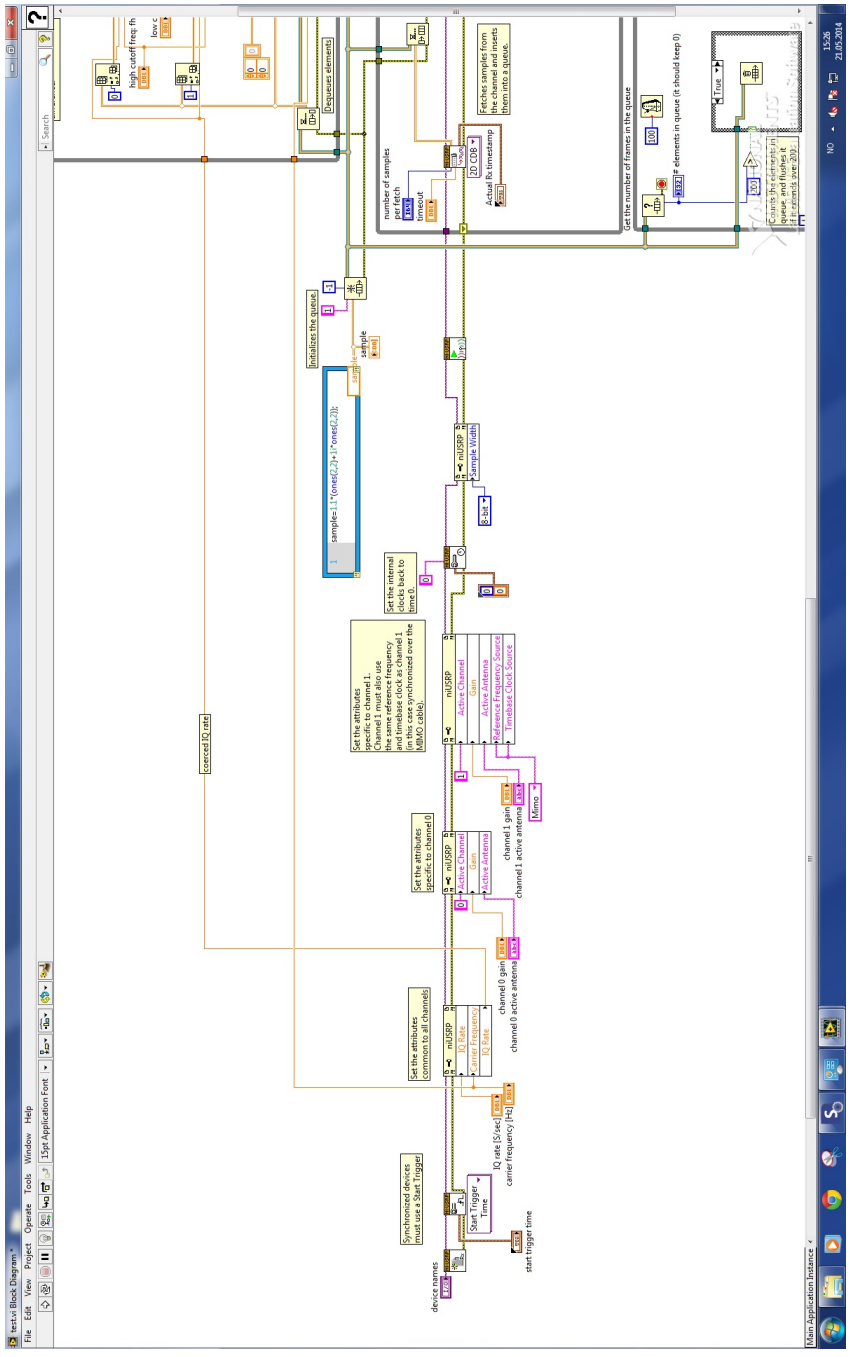

Figure 8.3: Complete VI of finished code part 1

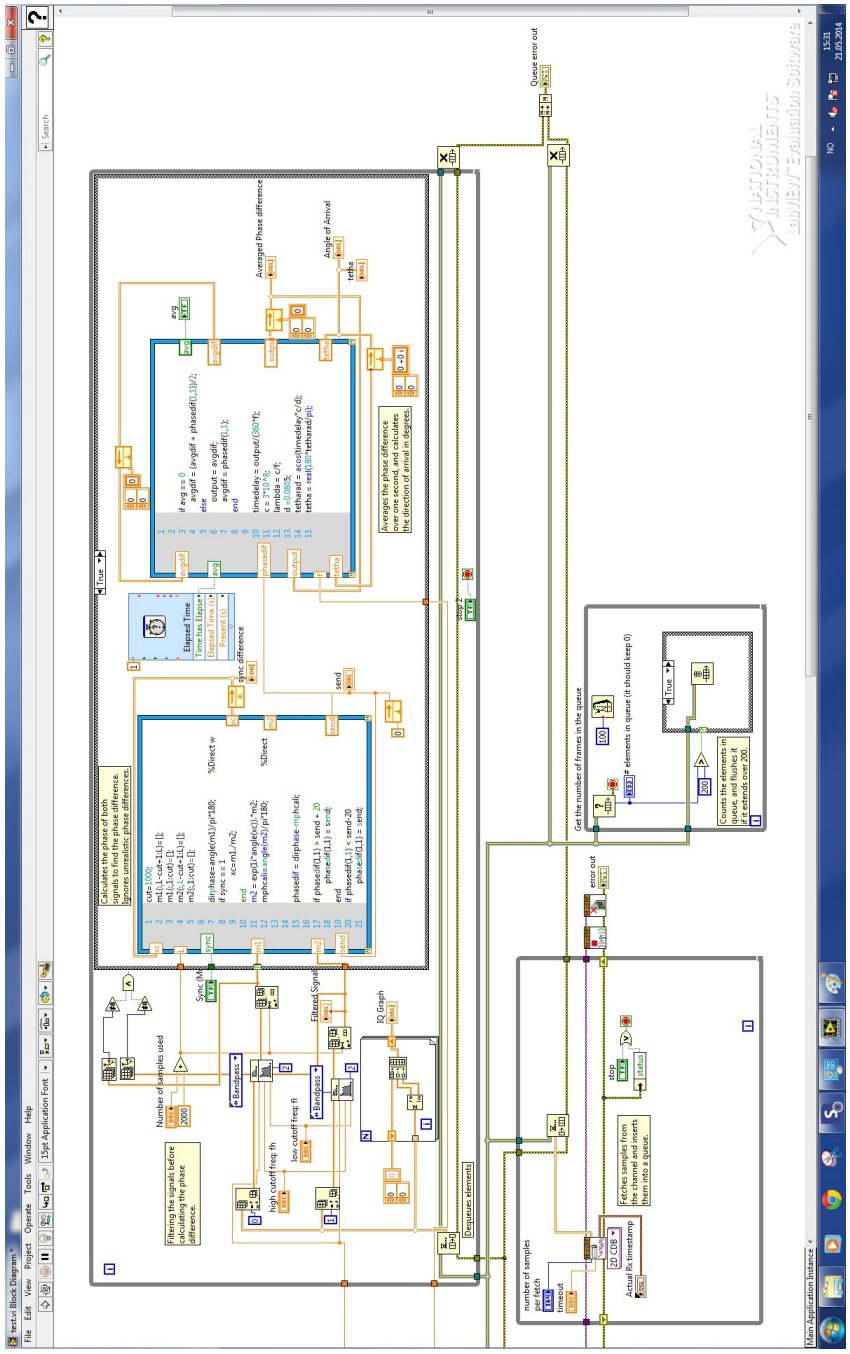

Figure 8.4: Complete VI of finsihed code part 2

LabVIEW code of the example niUSRP EX PSK Tx.vi

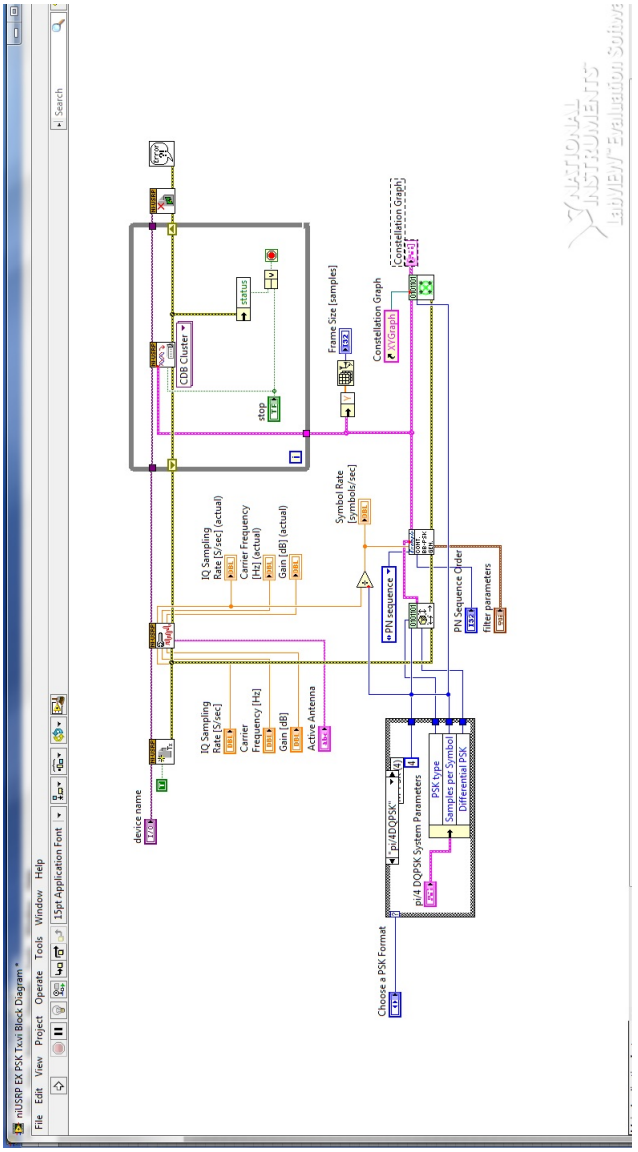

Figure 8.5: Complete VI of *niUSRP EX PSK Tx.vi* used for QPSK modulated signal generation

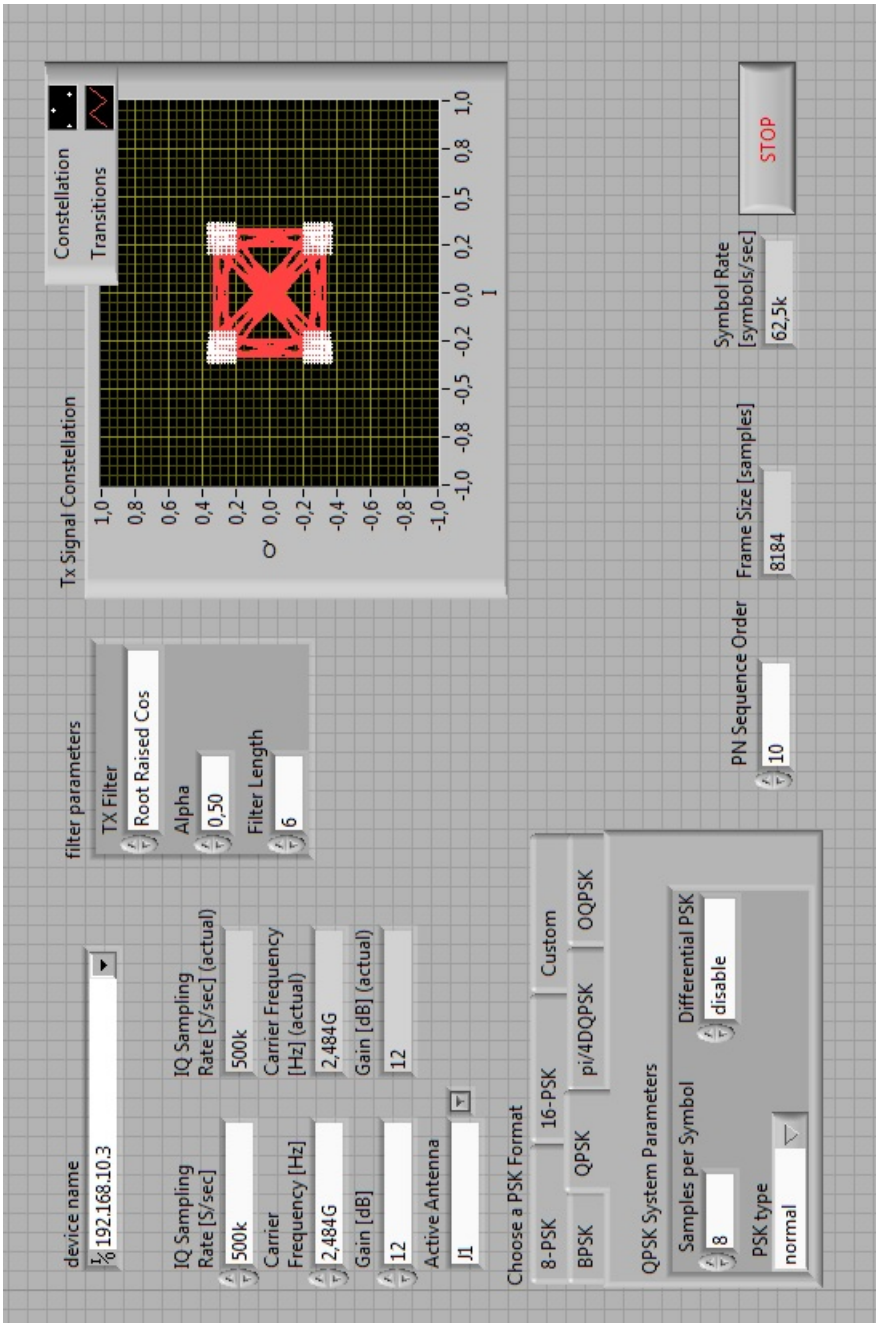

Figure 8.6: Front panel of *niUSRP EX PSK Tx.vi* used for QPSK modulated signal generation